Geophys. J. Int. (2005) **161,** 679–706 doi: 10.1111/j.1365-246X.2005.02553.x

On post-glacial sea level – II. Numerical formulation and comparative results on spherically symmetric models

Roblyn A. Kendall,[1] Jerry X. Mitrovica[1] and Glenn A. Milne[2]

[1]*Department of Physics, University of Toronto,* 60 *St George Street, Toronto, Ontario, Canada* M5S 1A7. *E-mail: rkendall@physics.utoronto.ca*
[2]*Department of Geological Sciences, University of Durham, Science Labs, South Road, Durham* DH1 3LE, *UK*

Accepted 2004 December 8. Received 2004 December 1; in original form 2004 June 4

SUMMARY

Theoretical approaches to computing gravitationally self-consistent sea-level changes in consequence of ice growth and ablation are comprised of two parts. The first is a mapping between variations in global sea level and changes in ocean height (required to define the surface load), and the second is a method for computing global sea-level change arising from an arbitrary surface loading. In Mitrovica & Milne (2003) (Paper I) we described a new, generalized mapping between sea-level change and ocean height that takes exact account of the evolution of shorelines associated with both transgression and regression cycles and time-dependent marine-based ice margins. The theory is valid for any earth model. In this paper we extend our previous work in three ways. First, we derive an efficient, iterative numerical algorithm for solving the generalized sea-level equation. Secondly, we consider a special case of the new sea-level theory involving spherically symmetric earth models. Specifically, we combine our iterative numerical formulation with viscoelastic Love number theory to derive an extended pseudo-spectral algorithm for solving the new sea-level equation. This algorithm represents an extension of earlier methods developed for the fixed-shoreline case to precisely incorporate shoreline migration processes. Finally, using this special case, we quantitatively assess errors incurred in previous efforts to extend the traditional (fixed shoreline) sea-level equation of Farrell & Clark (1976) to treat time-dependent shorelines. We find that the approximations adopted by Johnston (1993) and Milne (1998) to treat transgression and regression at shorelines introduce negligible ($\sim$1 per cent) error into predictions of post-glacial relative sea-level histories. In contrast, the errors associated with the Peltier (1994) sea-level equation are an order of magnitude larger, and comparable to the error incurred using the traditional sea-level theory. Furthermore, our numerical tests verify the high accuracy of the Milne (1998) approximation for treating the influence of grounded, marine-based ice.

Key words: glacial rebound, sea level.

1 INTRODUCTION

Predicting gravitationally self-consistent sea-level changes driven by the melting of ice sheets on a deformable earth is a complex undertaking. Under the assumption of an equilibrium, or hydrostatic, theory (e.g. Dahlen 1976), the sea-level redistribution will be governed by the gravitational field of the planet, since the sea surface is constrained to remain on an equipotential. However, this field is, in turn, perturbed by the redistribution of ocean mass, both through the direct attraction of the total (ice plus ocean) surface mass load and by solid earth deformations driven by this mass loading. As a further complexity, load-induced perturbations to the rotation vector of the planet will also have an impact on sea level, both through the re-orientation of the rotational potential and the deformation that results from this re-orientation. In addition, the ocean loading is defined by the local geometry of the shorelines, which will evolve as sea levels rise and fall or as grounded marine-based ice advances or retreats.

Farrell & Clark (1976), henceforth FC1976, provided an elegant theoretical framework for predicting gravitationally self-consistent, post-glacial sea-level changes, and it remains a standard reference in modern analyses of the glacial isostatic adjustment (GIA) process. The 'sea-level equation' they derived may be decomposed into two distinct (but coupled) components, each based on independent underlying assumptions. First, they outlined a Green's function approach to computing global sea-level changes driven by a surface mass load comprised of ice and ocean height changes. This approach was ultimately based on the viscoelastic surface load Love number theory developed by Peltier (1974), and thus assumed a spherically symmetric (i.e. radially stratified), linear viscoelastic, non-rotating earth model. Secondly, throughout

the glacial cycle they computed ocean height changes (i.e. one component of the surface mass load) from global sea-level changes by simply projecting the latter on to the geometry of the present-day oceans. That is, they assumed no grounded marine-based ice and shorelines fixed in time (or, more physically, shorelines characterized by steep vertical cliffs).

The initial implementation of the FC1976 theory was based on a space-domain calculation of the required convolutions, where ocean and ice geometries were discretized using circular discs (e.g. Peltier & Andrews 1976; Wu & Peltier 1983). Mitrovica & Peltier (1991) developed both a spectral and an iterative, pseudo-spectral solution to the FC1976 sea-level equation; the latter, which permits extremely high harmonic truncation levels (and thus spatial resolution), has become the standard approach within the GIA community. This pseudo-spectral algorithm performs all calculations in the spectral domain with the exception of the spatial projection required to map global sea-level changes into ocean height changes.

In recent years, renewed interest in the problem of post-glacial sea-level changes has led to improvements in both components of the FC1976 theory.

In the context of spherically symmetric earth models, the Green's function formulation for computing global sea-level changes associated with an ice and ocean load forcing has been augmented to include the impact of a time-dependent rotation vector (e.g. Han & Wahr 1989; Bills & James 1996; Milne & Mitrovica 1996, 1998a; Peltier 1998a; Milne *et al.* 2001). In this regard, Milne & Mitrovica (1996) were the first to describe a theory that incorporates both the direct and deformational components of the rotational 'disturbing' potential into a gravitationally self-consistent sea-level theory. More recently, a number of independent groups have developed finite-element numerical algorithms that abandon the assumption of spherical symmetry and permit one to compute the gravitational and solid surface response of spherical earth models characterized by arbitrary 3-D variations in visco-elastic structure (e.g. Wu & van der Wal 2003; Zhong *et al.* 2003; Latychev *et al.* 2005). Spectral finite-element codes are also being developed for this purpose (Martinec 2000). Moreover, finite-element methods have been used to explore the effects on GIA predictions of non-Newtonian rheology (Giunchi & Spada 2000).

Recent efforts to extend the second component of the FC1976 theory, the mapping between changes in global sea level and ocean height, to the case of a time-varying shoreline geometry, have been the subject of significant debate within the GIA community (see Mitrovica 2003 for a review of this debate). The two principal mechanisms leading to this evolution are shown, schematically, in Fig. 1. The left frame of the figure shows the landward migration of the shoreline in a zone of sea-level transgression, and the oceanward migration associated with regression. In this case, the change in ocean height between t_{j-1} and t_j cannot be be expressed as a simple projection of the global sea-level change during this time window on to a static shoreline, as in the FC1976 theory (which shoreline would one choose?). The right frame of the figure shows the change in the shoreline in consequence of the ablation of a grounded, marine-based ice sheet. In this case, the change in the ocean load height within the region vacated by the ice complex (the shaded region on the plot) is not governed by the change in global sea level across the time window, as is presumed in the FC1976 theory, but rather by the *total* distance between the top (sea surface) and bottom (solid surface) bounding fields of sea level.

Johnston (1993) (see also Lambeck & Nakada 1990), Peltier (1994) and Milne (1998) derived approximate, and distinct, versions of the governing sea-level equation for the case shown in Fig. 1(a). Johnston (1993) and Milne (1998) assumed that the change in ocean height between two successive time steps in the solution (i.e. from t_{j-1} to t_j in Fig. 1a) could be computed by projecting the global sea-level change across the same time interval on to an ocean geometry chosen for some representative time within that interval (in the case of Milne 1998 the choice was t_j). In contrast, Peltier (1994) computed the total ocean height change since the start of the loading (from, say, t_0 to t_j) by projecting the total global sea-level change since equilibrium on to the ocean geometry at the end of the interval.

In regard to the process in Fig. 1(b), Milne (1998) (see also Milne *et al.* 1999) coined the term 'water dumping' and he was the first to explicitly outline a method for including it in the sea-level theory. His method incorporated both the direct and deformational effects of the influx of water into the region vacated by the ablating, marine-based ice sheet, and he showed that both local and far-field relative sea-level histories would be impacted by the process. In subsequent work, Peltier (1998b) treated the process using a concept he called 'implicit ice'. He did not include the inundation in a revised sea-level equation, but rather computed, *a posteriori*, the total volume of water flux into such zones and the impact on eustatic sea-level changes. The ice-thickness equivalent of the water influx was the dominant contributor to the so-called

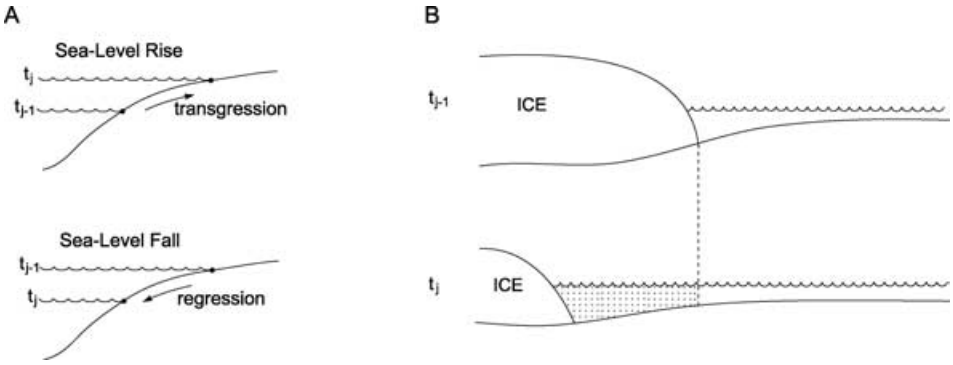

Figure 1. (a) A schematic illustration of shoreline evolution in the vicinity of a sea-level rise or fall. (b) An illustration of the water load influx into regions vacated by marine-based ice between $t = t_{j-1}$ and $t = t_j$. (After fig. 2 of Paper I).

'implicit' portion of the ice load. In the Peltier (1998b) formulation, it is assumed that the influx has no bearing on predicted relative sea-level histories.

In Mitrovica & Milne (2003), henceforth Paper I, we derived generalized and exact expressions linking global sea-level changes and ocean height changes. The relevant formulae were provided for changes taken across successive time increments in the sea-level solution and since the onset of loading. The new theory was used to derive analytic expressions for the error incurred in previous attempts to extend the sea-level theory to the case of an evolving shoreline (Figs 1a and b), and qualitative comparisons were made using a suite of schematic illustrations. The generalized theory makes no assumption in regard to the underlying earth model; however, its numerical implementation requires some means of predicting the response of the earth model to an external loading. In the case of spherically symmetric models, this requirement would involve the first (Green's function) component of the FC1976 theory, suitably extended to include rotational effects (Milne & Mitrovica 1996). In the case of more complex, 3-D earth models, one might invoke a finite-element formulation for computing the planetary response, although a perturbation theory does exist for treating this case within a normal mode framework (Tromp & Mitrovica 1999).

The present paper has two main goals. First, to derive a detailed form of the sea-level theory of Paper I that is suitable for numerical implementation on earth models of arbitrary complexity. Secondly, to apply this algorithm, in the special case of a spherically symmetric earth model, to quantitatively assess errors incurred in previous efforts to treat time-dependent shorelines in the governing sea-level theory. The paper has four parts. First, we very briefly review the main results in Paper I. Secondly, we derive a form of the theory that is amenable to an iterative numerical solution, including details associated with time-stepping, the treatment of grounded marine-based ice, conservation of surface load mass terms, and suitable 'first guesses' required for the various iterations. Thirdly, we consider the special case of spherically symmetric earth models, and present a new, 'extended' form of the pseudo-spectral approach (Mitrovica & Peltier 1991) that is designed for the theory of Paper I. Fourthly, we present results based on the extended pseudo-spectral procedure that assesses the relative accuracy of previous formulations for a suite of sites distinguished by their local shoreline geometry and distance from the major Late Pleistocene ice centres.

In a future companion paper (Part III), we combine the formulation described herein with a finite-element procedure described elsewhere (Latychev *et al.* 2005) to generate relative sea-level histories on earth models characterized by 3-D variations in mantle (including lithosphere) structure.

2 A GENERALIZED THEORY FOR POST-GLACIAL SEA-LEVEL CHANGE

In this section we briefly review the generalized sea-level theory described in Mitrovica & Milne (2003), which we will henceforth refer to as Paper I. Following Paper I, sea level is defined globally as the difference between the radial position of the geoid, G, and the solid surface, R (Fig. 2),

$$SL(\theta, \psi, t_j) = G(\theta, \psi, t_j) - R(\theta, \psi, t_j), \tag{1}$$

where θ is the colatitude and ψ is the longitude. We furthermore define topography as the inverse of this globally defined sea level,

$$T(\theta, \psi, t_j) = -SL(\theta, \psi, t_j). \tag{2}$$

The ocean depth is the projection of the global sea level (1) on to the ice-free oceans. To be consistent with the terminology used in Paper I, we will refer to the ocean depth as the ocean height, which may be written as

$$S(\theta, \psi, t_j) = SL(\theta, \psi, t_j) \cdot C(\theta, \psi, t_j)\beta(\theta, \psi, t_j), \tag{3}$$

where the ocean function is defined by (Fig. 2)

$$C(\theta, \psi, t_j) = \begin{cases} 1 & \text{if } SL(\theta, \psi, t_j) > 0 \\ 0 & \text{if } SL(\theta, \psi, t_j) \leq 0, \end{cases} \tag{4}$$

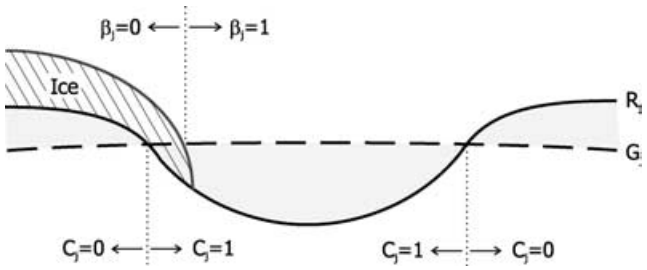

Figure 2. Schematic illustrating the bounding surfaces for globally defined sea level. Sea level is positive where $G > R$ and negative where $G < R$. Conversely, topography is positive where $R > G$ (land) and negative where $R < G$ (oceans). The fields C and β are defined in the text. We use the short form notation $R_j \equiv R(\theta, \psi, t_j)$, and likewise for the other fields shown.

and the β-field, prescribed from the input ice model, is given by (Fig. 2)

$$\beta(\theta, \psi, t_j) = \begin{cases} 1 & \text{where there is no grounded ice} \\ 0 & \text{where there is grounded ice.} \end{cases} \tag{5}$$

GIA-induced perturbations to the geoid and solid surfaces, which we will denote by ΔG and ΔR respectively, lead to variations in sea level. If we let $t = t_0$ denote the onset of loading, then the geoid at time t_j is given by the sum of the equilibrium geoid (prior to loading) and the GIA-induced changes to the geoid since t_0 (and similarly for the solid surface),

$$\begin{aligned} G(\theta, \psi, t_j) &= G(\theta, \psi, t_0) + \Delta G(\theta, \psi, t_j), \\ R(\theta, \psi, t_j) &= R(\theta, \psi, t_0) + \Delta R(\theta, \psi, t_j). \end{aligned} \tag{6}$$

It follows from (1) and (6) that

$$SL(\theta, \psi, t_j) = SL(\theta, \psi, t_0) + \Delta SL(\theta, \psi, t_j), \tag{7}$$

where

$$\Delta SL(\theta, \psi, t_j) = \Delta G(\theta, \psi, t_j) - \Delta R(\theta, \psi, t_j). \tag{8}$$

It will be convenient when describing our numerical algorithm to split the geoid anomaly, ΔG, into two components,

$$\Delta G(\theta, \psi, t_j) = \Delta \mathcal{G}(\theta, \psi, t_j) + \frac{\Delta \Phi(t_j)}{g}, \tag{9}$$

where $\Delta \mathcal{G}$ is the spatially varying component, and $\Delta \Phi(t_j)/g$ is a spatially uniform shift in the geoid that we will ultimately constrain by invoking conservation of mass of the surface load. If we also define

$$\Delta \mathcal{SL}(\theta, \psi, t_j) = \Delta \mathcal{G}(\theta, \psi, t_j) - \Delta R(\theta, \psi, t_j), \tag{10}$$

then (8) can be written as

$$\Delta SL(\theta, \psi, t_j) = \Delta \mathcal{SL}(\theta, \psi, t_j) + \frac{\Delta \Phi(t_j)}{g}. \tag{11}$$

It also follows from (2) and (7) that

$$T(\theta, \psi, t_j) = T(\theta, \psi, t_0) - \Delta SL(\theta, \psi, t_j). \tag{12}$$

It will be useful in later derivations to write the initial topography in terms of present-day values. Using (12),

$$T(\theta, \psi, t_0) = T(\theta, \psi, t_p) + \Delta SL(\theta, \psi, t_p). \tag{13}$$

We will also be interested in changes in sea level (and its bounding surfaces) that occur over successive time steps in the sea-level solution, rather than across the total time elapsed since the start of loading. We may write

$$\begin{aligned} \delta G(\theta, \psi, t_j) &= G(\theta, \psi, t_j) - G(\theta, \psi, t_{j-1}) = \Delta G(\theta, \psi, t_j) - \Delta G(\theta, \psi, t_{j-1}) \\ \delta R(\theta, \psi, t_j) &= R(\theta, \psi, t_j) - R(\theta, \psi, t_{j-1}) = \Delta R(\theta, \psi, t_j) - \Delta R(\theta, \psi, t_{j-1}) \end{aligned} \tag{14}$$

and

$$\delta SL(\theta, \psi, t_j) = SL(\theta, \psi, t_j) - SL(\theta, \psi, t_{j-1}) = \Delta SL(\theta, \psi, t_j) - \Delta SL(\theta, \psi, t_{j-1}). \tag{15}$$

Obtaining expressions for changes in the ocean height, over the time since the start of loading or across successive time increments, is somewhat more involved since this height requires a projection on to the ice-free ocean geometry. In analogy with earlier equations, we can write

$$S(\theta, \psi, t_j) = \Delta S(\theta, \psi, t_j) + S(\theta, \psi, t_0). \tag{16}$$

Then, using (2), (3) and (7), one can derive the generalized sea-level equation (henceforth GSLE),

$$\begin{aligned} \Delta S(\theta, \psi, t_j) = {} & \Delta SL(\theta, \psi, t_j)\, C\,(\theta, \psi, t_j)\, \beta\,(\theta, \psi, t_j) \\ & - T(\theta, \psi, t_0)[C(\theta, \psi, t_j)\beta(\theta, \psi, t_j) - C(\theta, \psi, t_0)\beta(\theta, \psi, t_0)]. \end{aligned} \tag{17}$$

Eq. (17) indicates that the change in the ocean height from the start of loading ($t = t_0$) to $t = t_j$ equals the change in global sea level projected on to the area of the ocean that is ice free at $t = t_j$ minus a correction term involving the initial topography. The latter term is a projection of the initial topography field on to a zone that is non-zero in any location where the ice-free ocean geometry at $t = t_j$ differs from the geometry at t_0 (see Paper I).

The change in the ocean load between successive time steps in the sea-level solution (rather than since the start of loading) is defined as

$$\delta S(\theta, \psi, t_j) = S(\theta, \psi, t_j) - S(\theta, \psi, t_{j-1}). \tag{18}$$

Using (17), this can be expressed as

$$\begin{aligned} \delta S(\theta, \psi, t_j) = {} & -\Delta S(\theta, \psi, t_{j-1}) + \Delta SL(\theta, \psi, t_j)\, C(\theta, \psi, t_j)\, \beta(\theta, \psi, t_j) \\ & - T(\theta, \psi, t_0)[C(\theta, \psi, t_j)\beta(\theta, \psi, t_j) - C(\theta, \psi, t_0)\beta(\theta, \psi, t_0)]. \end{aligned} \tag{19}$$

The numerical algorithm described below will be derived on the basis of this second form of the GSLE.

Eqs (17) and (19) are integral equations since the ocean height change being solved for defines one component of the surface load necessary to compute the RHS of these equations. As in the classic case where the continent margins are fixed (Farrell & Clark 1976; Mitrovica & Peltier 1991), numerical solution of (17) or (19) generally requires an iteration within each time step to refine the first guess to the ocean height change, δS.

However, the solution to these generalized equations also requires a second iteration loop, since although we know the present-day values $T(\theta, \psi, t_p)$ and $C(\theta, \psi, t_p)$, we do not know *a priori* either initial value $T(\theta, \psi, t_0)$ or $C(\theta, \psi, t_0)$ (e.g. Peltier 1994). Thus, an iteration over the full glaciation-deglaciation cycle is required until convergence of the initial topography field, $T(\theta, \psi, t_0)$, is achieved. This iteration will be based on the relation (13).

2.1 Special cases

2.1.1 No marine ice

In the special case where marine ice does not exist, our expression governing the location of ice-free oceans reduces to

$$C(\theta, \psi, t_j)\beta(\theta, \psi, t_j) \Rightarrow C(\theta, \psi, t_j) \tag{20}$$

for all times t_j. The expression for the ocean height in (3) then reduces to the projection of the sea level on to the oceans, and the change in ocean height (17) simplifies to

$$\Delta S(\theta, \psi, t_j) = \Delta SL(\theta, \psi, t_j)C(\theta, \psi, t_j) - T(\theta, \psi, t_0)[C(\theta, \psi, t_j) - C(\theta, \psi, t_0)], \tag{21}$$

while (19) becomes

$$\begin{aligned}\delta S(\theta, \psi, t_j) = &-\Delta S(\theta, \psi, t_{j-1}) + \Delta SL(\theta, \psi, t_j)C(\theta, \psi, t_j)\\ &- T(\theta, \psi, t_0)[C(\theta, \psi, t_j) - C(\theta, \psi, t_0)].\end{aligned} \tag{22}$$

2.1.2 Fixed continent margins and no marine ice

By removing the time-dependence of the continent margins, we are essentially assuming ocean basins with cliffs at the shorelines, in which case,

$$C(\theta, \psi, t_0) = \cdots = C(\theta, \psi, t_j) = \cdots = C(\theta, \psi, t_p) = C(\theta, \psi). \tag{23}$$

The change in ocean height therefore reduces to the classic FC1976 form of the sea-level equation,

$$\Delta S(\theta, \psi, t_j) = \Delta SL(\theta, \psi, t_j)\, C(\theta, \psi). \tag{24}$$

Note, in this case the change in the ocean height is given by a simple projection of the change in sea level on to the oceans. Finally, for this same special case,

$$\delta S(\theta, \psi, t_j) = -\Delta S(\theta, \psi, t_{j-1}) + \Delta SL(\theta, \psi, t_j)\, C(\theta, \psi). \tag{25}$$

2.2 Approximations to the GSLE

Paper I described, in detail, previous efforts to extend (24) to include effects associated with shorelines that evolve as a consequence of local transgression or regression and/or variations in the geometry of grounded, marine-based ice (Fig. 1). Paper I also derived expressions for the error incurred in these previous approaches relative to the exact GSLE theory (17) or (19), and illustrated this error with a series of schematics. In this section we list the main results of this derivation.

2.2.1 No marine ice

Researchers at the Australian National University were the first to implement time-dependent continent margins into the sea-level equation (Lambeck & Nakada 1990; Johnston 1993). The Johnston (1993) sea-level equation, which we will denote by the superscript J, can be written as

$$\delta S^J(\theta, \psi, t_j) = [-\Delta SL(\theta, \psi, t_{j-1}) + \Delta SL(\theta, \psi, t_j)]\, C\big(\theta, \psi, t_j^*\big), \tag{26}$$

where t^* is chosen to be 'representative of the time interval $t_{j-1} < t < t_j$' (Johnston 1993, p. 618). Unless the choice of t_j^* is defined, the error in the ocean height change associated with this approximation cannot be quantified. The error is a function of the choice of t_j^*, the size of the time step and the topography in the region of shoreline migration.

Peltier (1994) incorporated a time-dependent continent margin into the solution for the change in ocean height *since equilibrium* by replacing $C(\theta, \psi)$ in the fixed margins case (24) with a time-dependent continent function,

$$\Delta S^P(\theta, \psi, t_j) = \Delta SL(\theta, \psi, t_j)\, C(\theta, \psi, t_j). \tag{27}$$

Comparing with our equation (21), we may write

$$\Delta S^P(\theta, \psi, t_j) = \Delta S(\theta, \psi, t_j) + T(\theta, \psi, t_0)[C(\theta, \psi, t_j) - C(\theta, \psi, t_0)]. \tag{28}$$

The second term on the RHS represents the error associated with the Peltier (1994) approximation.

Finally, Milne and colleagues (Milne & Mitrovica 1998b; Milne 1998; Milne *et al.* 1999) used a method similar to that of Johnston (1993) to incorporate a time-dependent continent margin into the solution of the sea-level equation. However, rather than projecting the sea-level change on to an ocean function 'representative of the time interval', Milne and colleagues project the sea-level change on to the ocean function computed for the end of the time increment. That is,

$$\delta S^M(\theta, \psi, t_j) = [-\Delta SL(\theta, \psi, t_{j-1}) + \Delta SL(\theta, \psi, t_j)]\, C(\theta, \psi, t_j). \tag{29}$$

Comparing with (21) above, one can show that

$$\delta S^M(\theta, \psi, t_j) = \delta S(\theta, \psi, t_j) + T(\theta, \psi, t_{j-1})[C(\theta, \psi, t_j) - C(\theta, \psi, t_{j-1})]. \tag{30}$$

The second term on the RHS represents the error associated with this method.

A schematic illustration of the geometry of the error incurred by the approximations (26), (27) and (29), are provided in figs. 5, 6, and 7, respectively, of Paper I.

2.2.2 Marine ice

Milne (1998) and Milne *et al.* (1999) incorporated the water influx associated with the melting of grounded marine ice during the deglaciation phase of the glacial cycle. Their sea-level equation can be expressed as

$$\begin{aligned}\delta S^M(\theta, \psi, t_j) = {} & [-\Delta SL(\theta, \psi, t_{j-1}) + \Delta SL(\theta, \psi, t_j)]\, C(\theta, \psi, t_j)\beta(\theta, \psi, t_j) \\ & - T(\theta, \psi, t_{j-1})\, C(\theta, \psi, t_j)[\beta(\theta, \psi, t_j) - \beta(\theta, \psi, t_{j-1})].\end{aligned} \tag{31}$$

Comparing this approximation with (19) yields, after some algebra,

$$\delta S^M(\theta, \psi, t_j) = \delta S(\theta, \psi, t_j) + T(\theta, \psi, t_{j-1})\beta(\theta, \psi, t_{j-1})[C(\theta, \psi, t_j) - C(\theta, \psi, t_{j-1})]. \tag{32}$$

The second term on the RHS represents the error associated with this approximation.

Researchers at the Australian National University have also incorporated the effects of marine-based ice into their sea-level solutions (e.g. Lambeck *et al.* 1998), although only recently have they provided details of their approach (the interested reader is referred to Lambeck *et al.* 2003).

Finally, Peltier (1998b) also considered the presence of evolving marine-based ice sheets. However, as described in the Introduction, he did not alter his governing equation (27) to account for the impact on local sea level of this evolution. Rather, he appears to have performed an *a posteriori* calculation which considered the integrated effect of the process (e.g. the influx of water into all regions vacated by ablating marine-based ice) on estimates of eustatic sea-level rise.

3 A NUMERICAL ALGORITHM FOR SOLVING THE GSLE

In deriving an algorithm for the solution of our GSLE, we will focus on the change in ocean height over successive time steps (19) rather than over the total change from equilibrium (17). This approach is consistent with most numerical implementations of sea-level theory, which are generally designed to solve for the ocean height change following each ice loading increment. We begin by adopting a short-form version of (19),

$$\delta S_j = -\Delta S_{j-1} + \Delta\mathcal{SL}_j C_j \beta_j + \frac{\Delta\Phi_j}{g} C_j \beta_j - T_0[C_j\beta_j - C_0\beta_0]. \tag{33}$$

where we have substituted (11) into (19). For clarity and brevity, we have denoted time $t = t_j$ by the subscript j and have dropped the explicit (θ, ψ)-dependence. In this case, we remind the reader that $\frac{\Delta\Phi_j}{g}$ is a spatially uniform shift in the geoid, and is therefore the only term in (33) with no (θ, ψ)–dependence.

As described above, (33) is an integral equation because $\Delta\mathcal{SL}_j$, $\Delta\Phi_j$ and C_j are all dependent on the ocean load δS_j. Writing this dependency out explicitly for $\Delta\mathcal{SL}_j$ yields

$$\delta S_j = -\Delta S_{j-1} + \Delta\mathcal{SL}_j\left(\delta I_{m\ 0\le m\le j};\ \delta S_{m\ 0\le m<j};\ \delta S_j\right) C_j\beta_j + \frac{\Delta\Phi_j}{g} C_j\beta_j - T_0[C_j\beta_j - C_0\beta_0], \tag{34}$$

where the dependence of $\Delta\mathcal{SL}_j$ on the ice load increments, δI_m, has also been included.

3.1 The iteration process

As described above, a solution to the integral sea-level equation (34) will ultimately require two iteration loops. Before outlining a detailed numerical algorithm for obtaining this solution, it will be useful to specify our basic nomenclature for the iteration loops and our adopted time stepping.

(1) The time steps, which we have denoted by the index j, will extend from $j = 0, N$. For $j = N$, time $t = t_p$ will be used interchangeably with t_N to denote the present-day.

(2) The 'inner' iteration, identified by index i, refers to the loop over a single time step in which the ocean height increment $\delta S^i(\theta, \psi, t_j)$ is refined until convergence is achieved. We will refer to a converged value using the index $i = \infty$, $\delta S^{i=\infty}(\theta, \psi, t_j)$.

(3) The 'outer' iteration, identified by index k, refers to the loop over the full glaciation-deglaciation cycle. This loop is repeated until convergence of the initial topography field is achieved, $T^{k=\infty}(\theta, \psi, t_0)$.

(4) Any nth iterate value (whether it refers to the inner or outer iteration listed above) refers to a value that is computed within the nth cycle through the iteration loop. The zeroth iterate, $x^{n=0}$, is a first guess to a value that will then be recalculated during the first iteration through the cycle.

(5) During the (ith, kth) iteration at $t = t_j$, a parameter or field will be treated as known if it was computed at an earlier time step, $t < t_j$, or if it was computed during a prior iteration step (see below).

In defining the iteration procedure, the following variables will be superscripted as indicated:

$\delta S^{i,k}(\theta, \psi, t_j)$ $\quad \Delta S^{i,k}(\theta, \psi, t_j)$ $\quad \Delta\Phi^{i,k}(t_j)$

$\Delta\mathcal{SL}^{i,k}(\theta, \psi, t_j)$ $\quad T^k(\theta, \psi, t_j)$ $\quad C^k(\theta, \psi, t_j)$

Our numerical solution of (34) is then based on the adoption of the following iteration scheme (in both i and k),

$$\delta S_j^{i,k} = -\Delta S_{j-1}^{i=\infty,k} + \Delta\mathcal{SL}_j^{i-1,k}\left(\begin{matrix}\delta I_m \\ 0\le m\le j\end{matrix}; \begin{matrix}\delta S_m^{i=\infty,k} \\ 0\le m<j\end{matrix}; \delta S_j^{i-1,k}\right) C_j^{k-1}\beta_j + \frac{\Delta\Phi_j^{i-1,k}}{g} C_j^{k-1}\beta_j - T_0^{k-1}\left[C_j^{k-1}\beta_j - C_0^{k-1}\beta_0\right]. \tag{35}$$

The first term on the RHS of (35) represents the (negative of the) predicted change in the ocean height from the start of the loading to a time $t = t_{j-1}$. During the kth iteration through the glacial cycle, this quantity is assumed known from the convergence of the solution at the time step prior to $t = t_j$ (hence $i = \infty$). In the expression for $\Delta\mathcal{SL}_j^{i-1,k}$, within the second term on the RHS, the ice increments are known *a priori* from the input ice history. Furthermore, the kth iterate ocean height increments, δS_m, for $m < j$, are known from the convergence of the i-iteration at all previous time steps (hence $i = \infty$). During the kth iteration, the ocean function, C_j, and the initial topography, T_0, are known from results of the last iteration through the full glacial cycle, hence the superscript $k - 1$. The equations governing these quantities, in our iteration counter format, are given below. The (spatially invariant) quantity $\Delta\Phi_j^{i-1,k}$ may be obtained by invoking conservation of mass in the total surface (ice plus water) load. In this case, we multiply (35) by the density of water, ρ_{W}, integrate over the entire surface of the earth (denoted by Ω), and solve for $\Delta\Phi_j^{i-1,k}$ to obtain

$$\frac{\Delta\Phi_j^{i-1,k}}{g} = -\frac{1}{\mathcal{A}_j^{k-1}}\frac{\rho_{\mathrm{I}}}{\rho_{\mathrm{W}}}\iint_\Omega \Delta I_j\, d\Omega - \frac{1}{\mathcal{A}_j^{k-1}}\iint_\Omega \Delta\mathcal{SL}_j^{i-1,k}\left(\begin{matrix}\delta I_m \\ 0\le m\le j\end{matrix}; \begin{matrix}\delta S_m^{i=\infty,k} \\ 0\le m<j\end{matrix}; \delta S_j^{i-1,k}\right) C_j^{k-1}\beta_j\, d\Omega + \frac{1}{\mathcal{A}_j^{k-1}}\iint_\Omega T_0^{k-1}\left[C_j^{k-1}\beta_j - C_0^{k-1}\beta_0\right] d\Omega, \tag{36}$$

where ρ_{I} is the density of ice. Furthermore, $\mathcal{A}_j$, given by

$$\mathcal{A}_j^{k-1} = \iint_\Omega C_j^{k-1}\beta_j\, d\Omega, \tag{37}$$

is the area of the ice-free oceans at time t_j, and is based on the ocean function obtained from the previous iteration through the glacial cycle.

We now have all the components necessary to update $\delta S_j^{i-1,k}$ to $\delta S_j^{i,k}$ via (35). Specifically, we begin with a first guess, $\delta S_j^{i=0,k}$, and then use (36) and then (35) to compute the improved field $\delta S_j^{i=1,k}$. We then increase the iteration counter by one, and proceed through the i-loop until convergence is achieved, $\delta S_j^{i=\infty,k}$. This process is repeated for the next time step, t_{j+1}, and we continue in this way until $j = N$ (or equivalently, $t = t_p$).

By (35), we see that in order to proceed to the $k + 1$ iteration through the glacial cycle, we will require values for the kth iterate topography fields T_j^k, from which the kth iterate ocean functions C_j^k can be calculated. Using (13), the initial topography can be calculated from the known present-day topography $T(t_p)$ and the calculated change in sea level,

$$T_0^k = T(t_p) + \Delta SL_p^{i=\infty,k}. \tag{38}$$

The kth-iterate topography fields are generated by substituting (38) into (12),

$$T_j^k = T(t_p) + \Delta SL_p^{i=\infty,k} - \Delta SL_j^{i=\infty,k} \tag{39}$$

for $j = 1, N$. Using (2) and (4), the kth-iterate ocean functions are given by,

$$C_j^k = \begin{cases} 1 & \text{if } T_j^k < 0, \\ 0 & \text{if } T_j^k \geq 0. \end{cases} \tag{40}$$

Eqs (38)–(40) complete the kth iteration through the full glacial cycle and permit one to move on to the next iterate pass through the full glacial cycle and computation of the change in ocean height, $\delta S_j^{i,k+1}$. The entire process is repeated until convergence of the initial topography field is achieved, $T_0^{k=\infty}$. Clearly, by (38), this is ultimately governed by the convergence of the sea-level change $\Delta SL_p^{i=\infty,k=\infty}$.

Eqs (35), (36), (37), (38), (40) and (5) provide the basis for a numerical implementation of the GSLE (19). In the next section we introduce a small revision to this system of equations to account for a check on the input ice load.

3.2 The iteration process - 2: A check for grounded ice

Up to this point, we have assumed that the marine component of the input ice load is grounded. This assumption must be verified because, in practice, marine ice that is not grounded will not alter the ocean height upon melting.

Following Milne (2002), the marine ice load, defined as that portion of $I(\theta, \psi, t_j)$ located where $C(\theta, \psi, t_j) = 1$, will be grounded wherever

$$I(\theta, \psi, t_j) > |T(\theta, \psi, t_j)| \frac{\rho_{\rm w}}{\rho_{\rm i}}. \tag{41}$$

We can define a revised ice load, $I^*(\theta, \psi, t_j)$, composed only of land-based ice and grounded marine ice. That is, the ice load must satisfy the following grounding criteria,

$$I^*(\theta, \psi, t_j) = \begin{cases} I(\theta, \psi, t_j) & \text{where } C(\theta, \psi, t_j) = 0 \\ I(\theta, \psi, t_j) & \text{where } C(\theta, \psi, t_j) = 1 \textbf{ and } I(\theta, \psi, t_j) > |T(\theta, \psi, t_j)| \frac{\rho_{\rm w}}{\rho_{\rm i}} \\ 0 & \text{elsewhere.} \end{cases} \tag{42}$$

Since I^* depends on the topography field, the ice field will need to be updated after each iteration through the glacial cycle. Using the notation introduced in the last section, we write

$$I_j^{*k} = \begin{cases} I_j & \text{where } C_j^k = 0 \\ I_j & \text{where } C_j^k = 1 \textbf{ and } I_j > |T_j^k| \frac{\rho_{\rm w}}{\rho_{\rm i}} \\ 0 & \text{elsewhere.} \end{cases} \tag{43}$$

Furthermore, the $\beta-$field defined by (5) can be specified as

$$\beta_j^k = \begin{cases} 1 & \text{where } I_j^{*k} = 0 \\ 0 & \text{elsewhere.} \end{cases} \tag{44}$$

Using (43) and (44), the governing equations (35), (36) and (37) are updated to

$$\begin{aligned} \delta S_j^{i,k} = & -\Delta S_{j-1}^{i=\infty,k} + \Delta \mathcal{SL}_j^{i-1,k} \left(\begin{matrix} \delta I_m^{*k-1} \\ 0 \leq m \leq j \end{matrix} ; \begin{matrix} \delta S_m^{i=\infty,k} \\ 0 \leq m < j \end{matrix} ; \delta S_j^{i-1,k} \right) C_j^{k-1} \beta_j^{k-1} \\ & + \frac{\Delta \Phi_j^{i-1,k}}{g} C_j^{k-1} \beta_j^{k-1} - T_0^{k-1} \left[C_j^{k-1} \beta_j^{k-1} - C_0^{k-1} \beta_0^{k-1} \right], \end{aligned} \tag{45}$$

$$\begin{aligned} \frac{\Delta \Phi_j^{i-1,k}}{g} = & -\frac{1}{\mathcal{A}_j^{k-1}} \frac{\rho_{\rm i}}{\rho_{\rm w}} \iint_\Omega \Delta I_j^{*k-1} d\Omega \\ & - \frac{1}{\mathcal{A}_j^{k-1}} \iint_\Omega \Delta \mathcal{SL}_j^{i-1,k} \left(\begin{matrix} \delta I_m^{*k-1} \\ 0 \leq m \leq j \end{matrix} ; \begin{matrix} \delta S_m^{i=\infty,k} \\ 0 \leq m < j \end{matrix} ; \delta S_j^{i-1,k} \right) C_j^{k-1} \beta_j^{k-1} d\Omega \\ & + \frac{1}{\mathcal{A}_j^{k-1}} \iint_\Omega T_0^{k-1} \left[C_j^{k-1} \beta_j^{k-1} - C_0^{k-1} \beta_0^{k-1} \right] d\Omega, \end{aligned} \tag{46}$$

and

$$\mathcal{A}_j^{k-1} = \iint_\Omega C_j^{k-1} \beta_j^{k-1} d\Omega. \tag{47}$$

Eqs (45)–(47) define an iterative procedure for the final form of our GSLE. This system of equations is completed by the check on grounded ice, (43), which leads to the definition of the β-field (44). Finally, (38) provides the relationship between the computed total sea-level change at the present-day and the initial topography, within the kth iteration, while (39) and (40) provide a simple algorithm for computing the kth iterate ocean function.

3.3 Zeroth iterate values

In order to numerically implement eqs (45)–(47), we need to specify the zeroth iterate values, or first guesses to $T_j^{k=0}$, $C_j^{k=0}$, $\delta I_j^{*k=0}$, $\beta_j^{k=0}$ and $\delta S_j^{i=0,k}$.

3.3.1 First guess $k = 0$

To start the first k-loop, that is, the first pass through the full glacial cycle, we require first guesses $T_j^{k=0}$, $C_j^{k=0}$, $\delta I_j^{*k=0}$ and $\beta_j^{k=0}$. In this case, we simply let the set of $N + 1$ topography fields be equivalent to the present-day value,

$$T_j^{k=0} = T(t_p) \qquad j = 0, N \tag{48}$$

and thus

$$C_j^{k=0} = C_p \qquad j = 0, N. \tag{49}$$

From (40),

$$C_p = \begin{cases} 1 & \text{if } T(t_p) < 0 \\ 0 & \text{elsewhere.} \end{cases} \tag{50}$$

Continuing, (43) and (44) become

$$I_j^{*k=0} = \begin{cases} I_j & \text{where } C_p = 0 \\ I_j & \text{where } C_p = 1 \textbf{ and } I_j > |T(t_p)| \frac{\rho_{\mathrm{W}}}{\rho_{\mathrm{I}}} \\ 0 & \text{elsewhere} \end{cases} \tag{51}$$

and

$$\beta_j^{k=0} = \begin{cases} 1 & \text{where } I_j^{*k=0} = 0 \\ 0 & \text{elsewhere.} \end{cases} \tag{52}$$

We may therefore write the $k = 1$ version of the sea-level equation (45) as

$$\begin{aligned} \delta S_j^{i,k=1} = &-\Delta S_{j-1}^{i=\infty,k=1} + \Delta \mathcal{SL}_j^{i-1,k=1} \left(\delta I_{\substack{m \\ 0 \le m \le j}}^{*k=0}; \delta S_{\substack{m \\ 0 \le m < j}}^{i=\infty,k=1}; \delta S_j^{i-1,k=1} \right) C_p \beta_j^{k=0} \\ &+ \frac{\Delta \Phi_j^{i-1,k=1}}{g} C_p \beta_j^{k=0} - T(t_p) C_p \left[\beta_j^{k=0} - \beta_0^{k=0} \right]. \end{aligned} \tag{53}$$

Furthermore, the $k = 1$ versions of (46) and (47) are

$$\begin{aligned} \frac{\Delta \Phi_j^{i-1,k=1}}{g} = &-\frac{1}{\mathcal{A}_j^{k=0}} \frac{\rho_{\mathrm{I}}}{\rho_{\mathrm{W}}} \iint_\Omega \Delta I_j^{*k=0} d\Omega \\ &- \frac{1}{\mathcal{A}_j^{k=0}} \iint_\Omega \Delta \mathcal{SL}_j^{i-1,k=1} \left(\delta I_{\substack{m \\ 0 \le m \le j}}^{*k=0}; \delta S_{\substack{m \\ 0 \le m < j}}^{i=\infty,k=1}; \delta S_j^{i-1,k=1} \right) C_p \beta_j^{k=0} d\Omega \\ &+ \frac{1}{\mathcal{A}_j^{k=0}} \iint_\Omega T(t_p) C_p \left[\beta_j^{k=0} - \beta_0^{k=0} \right] d\Omega, \end{aligned} \tag{54}$$

and

$$\mathcal{A}_j^{k=0} = \iint_\Omega C_p \beta_j^{k=0} \, d\Omega. \tag{55}$$

3.3.2 First guess $i = 0$

To start each i-loop, that is, to initiate the (inner) iteration loop at a specific time increment, we require a first guess, $\delta S_j^{i=0,k}$. In this case, we specify two schemes, depending on the k value.

For the $k = 1$ case, we have fixed shorelines, but the extent of the oceans may be limited by the presence of grounded marine ice. Traditionally, the $i = 0$ guess to the sea-level equation is the so-called eustatic rise; that is, the meltwater is assumed to distribute evenly within the available ocean geometry. Thus, in the absence of marine ice, the first guess would be based on the purely eustatic rise depicted in Fig. 3(a). However, the general ($k = 1$) case when marine ice is present is better described by Fig. 3(b), where inundation into a zone of ice ablation between t_{j-1} and t_j also occurs. For this case, we can write

$$\delta S_j^{i=0,k=1} = \delta h_j C_p \beta_{j-1}^{k=0} - T_p C_p \left[\beta_j^{k=0} - \beta_{j-1}^{k=0} \right], \tag{56}$$

where δh is a uniform change in ocean height (that is, δh has no (θ, ψ)-dependence).

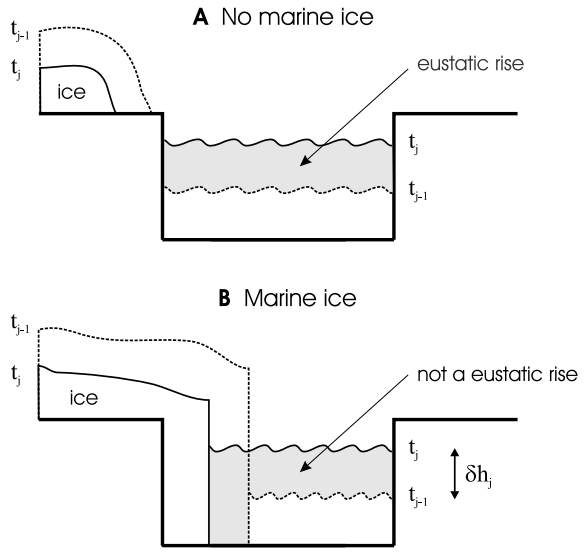

Figure 3. Schematic illustrating the ocean height change in (a) the presence of a fixed shoreline, where the rise is eustatic, and (b) in the presence of a receding marine ice complex, where in addition to the uniform rise in ocean height, water also flows into the region previously occupied by the marine ice.

The parameter δh_j may be constrained by invoking conservation of mass of the surface load (ice plus water) increment. Applying this constraint to (56) ultimately yields,

$$\delta h_j = -\frac{\rho_{\rm i}}{\rho_{\rm w}} \frac{1}{\mathcal{A}_{j-1}^{k=0}} \iint_\Omega \delta I_j^{*k=0} d\Omega + \frac{1}{\mathcal{A}_{j-1}^{k=0}} \iint_\Omega T_p C_p \left[\beta_j^{k=0} - \beta_{j-1}^{k=0}\right] d\Omega, \tag{57}$$

where, following (55), $\mathcal{A}_{j-1}^{k=0}$ is the area of the present-day ocean basins that would be free of grounded ice in the presence of the t_{j-1} model ice load. Substituting (57) into (56), the first guess to be used in the $i-$loop of (53) is given by

$$\begin{aligned}\delta S_j^{i=0,k=1} = {} & C_p \frac{\beta_{j-1}^{k=0}}{\mathcal{A}_{j-1}^{k=0}} \iint_\Omega \left(-\frac{\rho_{\rm i}}{\rho_{\rm w}} \delta I_j^{*k=0} + T_p C_p \left[\beta_j^{k=0} - \beta_{j-1}^{k=0}\right] \right) d\Omega \\ & - T_p C_p \left[\beta_j^{k=0} - \beta_{j-1}^{k=0}\right].\end{aligned} \tag{58}$$

Finally, we must also determine a first guess for $\delta S_j^{i=0,k>1}$. For the $k > 1$ iterations through the glacial cycle, the continent margins are treated as time dependent. We may now simply use the change in ocean height determined in the previous glacial cycle as a first guess. That is, for $k > 1$, the first guess in the $i-$loop of (45) is simply

$$\delta S_j^{i=0,k>1} = \delta S_j^{i=\infty,k-1}. \tag{59}$$

The input $\delta S_j^{i=0,k>1}$ are not eustatic, and will also account for the sloping continent margins.

To summarize, the equations governing our numerical (iterative) solution to the generalized sea-level problem are given by (45)–(47). Solution to the integral equation (45) requires two iteration loops. The 'inner' iteration (denoted by superscript i) occurs within each time step to refine the first guess to the ocean height change. The 'outer' iteration (denoted by superscript k) occurs over the full glacial cycle to refine the initial topography field. Eqs (48), (49), (52), (58) and (59) provide the input required for the first iterations through these loops. In the next section, we turn our attention to the implementation of the above equations in the case of spherically symmetric earth models.

In Appendix A we provide special cases for the above (iterative) equations in situations where there is no marine based ice (22) and, additionally, the continent margins are fixed (25).

4 SOLVING THE GSLE ON SPHERICALLY SYMMETRIC EARTH MODELS

The generalized sea-level equation and numerical algorithm defined by eqs (45)–(47) are valid for any 3-D viscoelastic earth model. In this regard, the equations are solvable once a formalism for computing $\Delta\mathcal{SL}_j$ or, via (10), the spatially varying gravitational potential perturbation and radial displacement, ΔG_j and ΔR_j respectively, is prescribed for a given set of surface mass load increments. For 3-D earth models, for example, numerical methods are independently being developed by several groups for this purpose.

In this section, we turn to the special case of a spherically symmetric earth model. Under this assumption, predictions of the gravitational potential perturbation and radial displacement have generally been performed using the (spectral) viscoelastic Love number theory of Peltier (1974). Furthermore, Mitrovica & Peltier (1991) developed a pseudo-spectral numerical algorithm in the case of fixed continent margins with no marine-based ice (our eqs A8 and A9). In the following, we provide an extended form of the pseudo-spectral formulation suitable for the generalized sea-level theory (45)–(47). This derivation will provide a complete description for the numerical solution of (45)–(47) for the case of spherically symmetric models. We begin by reviewing notation we adopt in introducing spectral quantities.

4.1 Notation

Any field defined on the surface of a sphere can be decomposed into a series of spherical harmonics,

$$\chi(\theta, \psi, t) = \sum_{\ell=0}^{\infty} \sum_{m=-\ell}^{\ell} \chi_{\ell m}(t) Y_{\ell m}(\theta, \psi), \tag{60}$$

where ℓ and m represent the spherical harmonic degree and order, respectively. We will normalize the spherical harmonic basis functions in the following manner,

$$\int\int_{sphere} Y_{\ell' m'}(\theta, \psi) Y^*_{\ell m}(\theta, \psi) \sin\theta \, d\theta \, d\psi = 4\pi \delta_{\ell' \ell} \delta_{m' m}, \tag{61}$$

where the asterisk denotes complex conjugation.

The spectral formulation used in combination with our iterative equations governing the sea-level solution requires numerous subscripts. To avoid confusion, we introduce a new notation as follows,

$$\chi^{i,k}(\theta, \psi, t_j) = \chi^{i,k}_j(\theta, \psi) = \sum_{\ell,m} [\chi_{\ell m}(t_j)]^{i,k} Y_{\ell m}(\theta, \psi). \tag{62}$$

The square brackets on the RHS denote a field subject to iterative improvement, with the corresponding iteration indices i and k superscripted *outside* the square brackets. To deal with the increasing number of subscripts, we now explicitly write out the time dependence of the spherical harmonic coefficients. Note that we have also introduced a shorthand notation for the double summation,

$$\sum_{\ell,m} \equiv \sum_{\ell=0}^{\infty} \sum_{m=-\ell}^{\ell}. \tag{63}$$

For fields that do not involve iterative refinement, the analogue to (62) will be

$$\chi(\theta, \psi, t_j) = \chi_j(\theta, \psi) = \sum_{\ell,m} \chi_{\ell m}(t_j) Y_{\ell m}(\theta, \psi). \tag{64}$$

4.2 An extended pseudo-spectral algorithm

The pseudo-spectral approach to solving the sea-level equation involves calculations in both the spectral and the space domains. Most calculations are performed spectrally, with the exception of the projections of any globally-defined field on to the ocean function; the latter are performed in the space domain.

For clarity, we introduce a new function $\mathcal{C}$ defined as

$$\mathcal{C}^k(\theta, \psi, t_j) = C^k(\theta, \psi, t_j) \cdot \beta^k(\theta, \psi, t_j), \tag{65}$$

which, as described above, has a value of unity over the (grounded) ice-free ocean and zero elsewhere. Using this new function, and the notations described above, we can rewrite the sea-level equation (45) in the spectral form

$$\begin{aligned}
\sum_{\ell,m} [\delta S_{\ell m}(t_j)]^{i,k} Y_{\ell m}(\theta, \psi) = &- \sum_{\ell,m} [\Delta S_{\ell m}(t_{j-1})]^{i=\infty,k} Y_{\ell m}(\theta, \psi) \\
&+ \left\{ \sum_{p,q} [\Delta \mathcal{SL}_{pq}(t_j)]^{i-1,k} Y_{pq}(\theta, \psi) + \left[\frac{\Delta \Phi(t_j)}{g} \right]^{i-1,k} Y_{00}(\theta, \psi) \right\} \\
&\times \left\{ \sum_{r,s} [\mathcal{C}_{rs}(t_j)]^{k-1} Y_{rs}(\theta, \psi) \right\} \\
&- \left\{ \sum_{p,q} [T_{pq}(t_0)]^{k-1} Y_{pq}(\theta, \psi) \right\} \times \left\{ \sum_{r,s} \left([\mathcal{C}_{rs}(t_j)]^{k-1} - [\mathcal{C}_{rs}(t_0)]^{k-1} \right) Y_{rs}(\theta, \psi) \right\},
\end{aligned} \tag{66}$$

where $Y_{00} = 1$ according to the normalization scheme (61).

We may define the projection

$$RO^{i-1,k}_j(\theta, \psi) = \left\{ \sum_{p,q} [\Delta \mathcal{SL}_{pq}(t_j)]^{i-1,k} Y_{pq}(\theta, \psi) \right\} \times \left\{ \sum_{r,s} [\mathcal{C}_{rs}(t_j)]^{k-1} Y_{rs}(\theta, \psi) \right\} \tag{67}$$

or, alternatively,

$$RO^{i-1,k}_j(\theta, \psi) = \Delta \mathcal{SL}^{i-1,k}_j(\theta, \psi) \mathcal{C}^{k-1}_j(\theta, \psi). \tag{68}$$

The spherical harmonic representation of the projection $RO_j(\theta, \psi)$ is given by

$$RO^{i-1,k}_j(\theta, \psi) = \sum_{\ell,m} [RO_{\ell m}(t_j)]^{i-1,k} Y_{\ell m}(\theta, \psi). \tag{69}$$

Similarly, we may define the projection

$$TO^{k-1}_j(\theta, \psi) = T^{k-1}_0(\theta, \psi) \left[\mathcal{C}^{k-1}_j(\theta, \psi) - \mathcal{C}^{k-1}_0(\theta, \psi) \right], \tag{70}$$

with a spherical harmonic representation given by

$$TO_j^{k-1}(\theta,\psi) = \sum_{\ell,m}[TO_{\ell m}(t_j)]^{k-1} Y_{\ell m}(\theta,\psi). \tag{71}$$

The sea-level equation (66) can then be rewritten as

$$\begin{aligned}\sum_{\ell,m}[\delta S_{\ell m}(t_j)]^{i,k} Y_{\ell m}(\theta,\psi) = &-\sum_{\ell,m}[\Delta S_{\ell m}(t_{j-1})]^{i=\infty,k} Y_{\ell m}(\theta,\psi)\\ &+\sum_{\ell,m}[RO_{\ell m}(t_j)]^{i-1,k} Y_{\ell m}(\theta,\psi)\\ &+\left[\frac{\Delta\Phi(t_j)}{g}\right]^{i-1,k}\sum_{\ell,m}[\mathcal{C}_{\ell m}(t_j)]^{k-1} Y_{\ell m}(\theta,\psi)\\ &-\sum_{\ell,m}[TO_{\ell m}(t_j)]^{k-1} Y_{\ell m}(\theta,\psi).\end{aligned} \tag{72}$$

We can rewrite (72) in terms of the individual spectral components,

$$\begin{aligned}[\delta S_{\ell m}(t_j)]^{i,k} = &-[\Delta S_{\ell m}(t_{j-1})]^{i=\infty,k} + [RO_{\ell m}(t_j)]^{i-1,k} + \left[\frac{\Delta\Phi(t_j)}{g}\right]^{i-1,k}[\mathcal{C}_{\ell m}(t_j)]^{k-1}\\ &-[TO_{\ell m}(t_j)]^{k-1}.\end{aligned} \tag{73}$$

To find the spectral equivalent of (46), we begin by applying (60) and (61) to (47) and find that

$$\mathcal{A}_j^{k-1} = 4\pi a^2[\mathcal{C}_{00}(t_j)]^{k-1}. \tag{74}$$

Similarly, the integral in the first term on the RHS of (46) can be written as

$$\iint_\Omega \Delta I_j^{*k-1}(\theta,\psi)d\Omega = 4\pi a^2\left[\Delta I_{00}^*(t_j)\right]^{k-1}. \tag{75}$$

Next, using (68)–(71), we can write

$$\iint_\Omega \Delta\mathcal{SL}_j^{i-1,k}(\theta,\psi)\mathcal{C}_j^{k-1}(\theta,\psi)d\Omega = 4\pi a^2[RO_{00}(t_j)]^{i-1,k} \tag{76}$$

and

$$\iint_\Omega T_0^{k-1}(\theta,\psi)\left[\mathcal{C}_j^{k-1}(\theta,\psi) - \mathcal{C}_0^{k-1}(\theta,\psi)\right]d\Omega = 4\pi a^2[TO_{00}(t_j)]^{k-1}. \tag{77}$$

Combining (74)–(77), the spectral form of (46) is given by

$$\left[\frac{\Delta\Phi(t_j)}{g}\right]^{i-1,k} = \frac{1}{\left[\mathcal{C}_{00}(t_j)\right]^{k-1}}\left(-\frac{\rho_{\rm I}}{\rho_{\rm W}}\left[\Delta I_{00}^*(t_j)\right]^{k-1} - [RO_{00}(t_j)]^{i-1,k} + [TO_{00}(t_j)]^{k-1}\right). \tag{78}$$

We will also require a spectral form for the ($i = 0$, $k = 1$) first guess to the ocean load increment, $\delta S_j^{i=0,k=1}$. The harmonic coefficients of (58) are given by

$$\begin{aligned}[\delta S_{\ell m}(t_j)]^{i=0,k=1} = &\frac{[\mathcal{C}_{\ell m}(t_{j-1})]^{k=0}}{[\mathcal{C}_{00}(t_{j-1})]^{k=0}}\left(-\frac{\rho_{\rm I}}{\rho_{\rm W}}\left[\delta I_{00}^*(t_j)\right]^{k=0} + \mathcal{T}_{00}(t_j) - \mathcal{T}_{00}(t_{j-1})\right)\\ &-(\mathcal{T}_{\ell m}(t_j) - \mathcal{T}_{\ell m}(t_{j-1})),\end{aligned} \tag{79}$$

where we have used $C^{k=0}(\theta,\psi,t) = C_p(\theta,\psi)$ and have defined the projection

$$\mathcal{T}_j(\theta,\psi) = T_0^{k=0}(\theta,\psi)\mathcal{C}_j^{k=0}(\theta,\psi) = T_p(\theta,\psi)\,C_p(\theta,\psi)\beta_j^{k=0}(\theta,\psi), \tag{80}$$

with spherical harmonic representation

$$\mathcal{T}_j(\theta,\psi) = \sum_{\ell,m}\mathcal{T}_{\ell m}(t_j)Y_{\ell m}(\theta,\psi). \tag{81}$$

From (59), the spectral form for the first guess in the $k > 1$ case is simply given by

$$[\delta S_{\ell m}(t_j)]^{i=0,k>1} = [\delta S_{\ell m}(t_j)]^{i=\infty,k-1}. \tag{82}$$

In order to determine whether convergence has been achieved for the inner *i*–iteration, we need to compute

$$\xi_j^{i,k} = \left|\frac{\sum_{\ell,m}\left|[\delta S_{\ell m}(t_j)]^{i,k}\right| - \sum_{\ell,m}\left|[\delta S_{\ell m}(t_j)]^{i-1,k}\right|}{\sum_{\ell,m}\left|[\delta S_{\ell m}(t_j)]^{i-1,k}\right|}\right|. \tag{83}$$

If $\xi_j^{i,k} < \epsilon_1$ (where ϵ_1 is typically taken to be $\sim 10^{-4}$), then

$$[\delta S_{\ell m}(t_j)]^{i,k} = [\delta S_{\ell m}(t_j)]^{i=\infty,k}, \tag{84}$$

otherwise, we set $i = i + 1$ and continue in the *i*-loop.

Note that once we have the converged value $\delta S_j^{i=\infty,k}$, we also have converged values $\Delta\mathcal{SL}_j^{i=\infty,k}$ and $\frac{\Delta\Phi_j^{i=\infty,k}}{g}$, and according to (11),

$$[\Delta SL_{\ell m}(t_j)]^{i=\infty,k} = [\Delta\mathcal{SL}_{\ell m}(t_j)]^{i=\infty,k} + \left[\frac{\Delta\Phi(t_j)}{g}\right]^{i=\infty,k}. \tag{85}$$

To complete the iteration through the glacial cycle, we check for convergence of the initial topography field,

$$\zeta_0^k = \left| \frac{\sum_{\ell,m} \left|[T_{\ell m}(t_0)]^k\right| - \sum_{\ell,m} \left|[T_{\ell m}(t_0)]^{k-1}\right|}{\sum_{\ell,m} \left|[T_{\ell m}(t_0)]^{k-1}\right|} \right|. \tag{86}$$

If $\zeta_0^k < \epsilon_2$ (where we will take $\epsilon_2 \sim 10^{-4}$), then we have convergence and

$$[T_{\ell m}(t_0)]^k = [T_{\ell m}(t_0)]^{k=\infty}, \tag{87}$$

otherwise, we set $k = k + 1$ and continue on to a next pass through the full glacial cycle.

4.2.1 A flowchart for the extended pseudo-spectral algorithm

The numerical implementation of the pseudo-spectral algorithm is summarized by the flowchart in Fig. 4 for a spherically symmetric earth model with time-dependent continent margins. The various steps in the flowchart refer to the corresponding equations in the text. The term 'pseudo-spectral' refers to the fact that the projections (65), (68) and (71), required as part of the sea-level equation (45), are not performed in the spectral domain (to do so would be a numerically intensive procedure). Rather, these projections are trivially performed in the space domain at the low numerical cost of synthesizing a small number of spatial fields from their spectral coefficients prior to the projection and then decomposing the product back into the spectral domain.

We have yet to specify the equations governing the computation of the field $\Delta\mathcal{SL}$ in the case of spherically symmetric earth models. Recall from (10) that $\Delta\mathcal{SL}$ is the difference between the total perturbation (i.e. since equilibrium) to the geoid position and the radial displacement driven by the surface loading. In the case of spherical symmetry, expressions for $\Delta\mathcal{SL}$ have been derived using viscoelastic Love number theory (Peltier 1974) for the case of both non-rotating (e.g. Farrell & Clark 1976; Mitrovica & Peltier 1991) and rotating (e.g. Milne & Mitrovica 1998a) earth models. In Appendix B we provide a brief summary of these derivations using the iterative notation required for the direct implementation of the extended pseudo-spectral algorithm.

5 RESULTS

We next present a suite of numerical results based on the implementation of the new generalized sea-level algorithm for spherically symmetric earth models outlined in Section 4. We have two goals in this section: First, to compare sea-level histories computed using the classic sea-level equation of FC1976 with results from the new theory at a geographically distributed set of sites. These sites are chosen to sample regions of both steep and shallow local shoreline geometry and varying proximity to ancient marine-based ice complexes. Secondly, and more importantly, to quantify errors introduced by previous algorithms designed to account for the shoreline migration effects shown in Fig. 1.

All calculations are based on an earth model characterized by an 80 km thick elastic lithosphere, upper and lower mantle viscosity of 5×10^{20} and 5×10^{21} Pa s, respectively, and the elastic and density structure of the seismic model PREM (Dziewonski & Anderson 1981). We solve the non-rotating form of the extended pseudo-spectral approach (i.e. Section 4.2 coupled with Appendix B1), with a truncation at spherical harmonic degree and order 256. When we discuss solutions based on the classic, FC1976 sea-level equation, we refer to solutions based on eqs A8–A10, completed with those in Appendix B1, and solved using the original pseudo-spectral algorithm (Mitrovica & Peltier 1991).

We will consider two different ice histories. The first is constructed by modifying the ICE-3G deglaciation model (Tushingham & Peltier 1991) to include a 90 kyr glaciation phase. This modification is accomplished by reversing the sign of the melting increments in ICE-3G and spacing them backwards in time prior to the last glacial maximum (LGM). Fig. 5 shows the extent of ice cover in the ICE-3G model at LGM (18 kyr BP in this model); it is clear from the figure that the model involves a significant marine-based component at LGM (e.g, Kara, Barents and East Siberian Seas, Hudson Bay, the Antarctic margin, etc.) It will also be instructive to consider a second ice history which involves no marine-based component. We have constructed such a history by setting up a series of parabolic continental ice domes in regions characterized by ICE-3G ice cover (henceforth the 'DISK' model); the mass history of these domes yields a eustatic sea-level change through the glacial cycle that follows the ICE-3G variation.

Fig. 6 shows predicted relative sea-level histories at six sites computed using the ICE-3G ice history, the earth model described above, and both the new and classic sea-level theories. The location of these six sites, as well as others discussed in this section, are shown in Fig. 5. The sites in Fig. 6 sample areas once covered by (Ottawa Island) or close to (Lark Harbour, Bar Harbor) marine-based ice, as well as far-field locations near continental margins (Mar del Plata, Cape York) and mid-ocean islands (Norfolk Island). Discrepancies exist at all sites, although the amplitude is a strong function of geographic location. It is clear, even from this small sample of results, that improvements embodied within the new sea-level theory are significant, although the detailed source of the various discrepancies is still unclear. For example, while the differential results at Ottawa Island are dominated by the water dumping mechanism, the analogous results at Mar del Plata are presumably due to some combination of the local improvement in the treatment of the ocean load and the integrated effect of changes in shoreline geometry

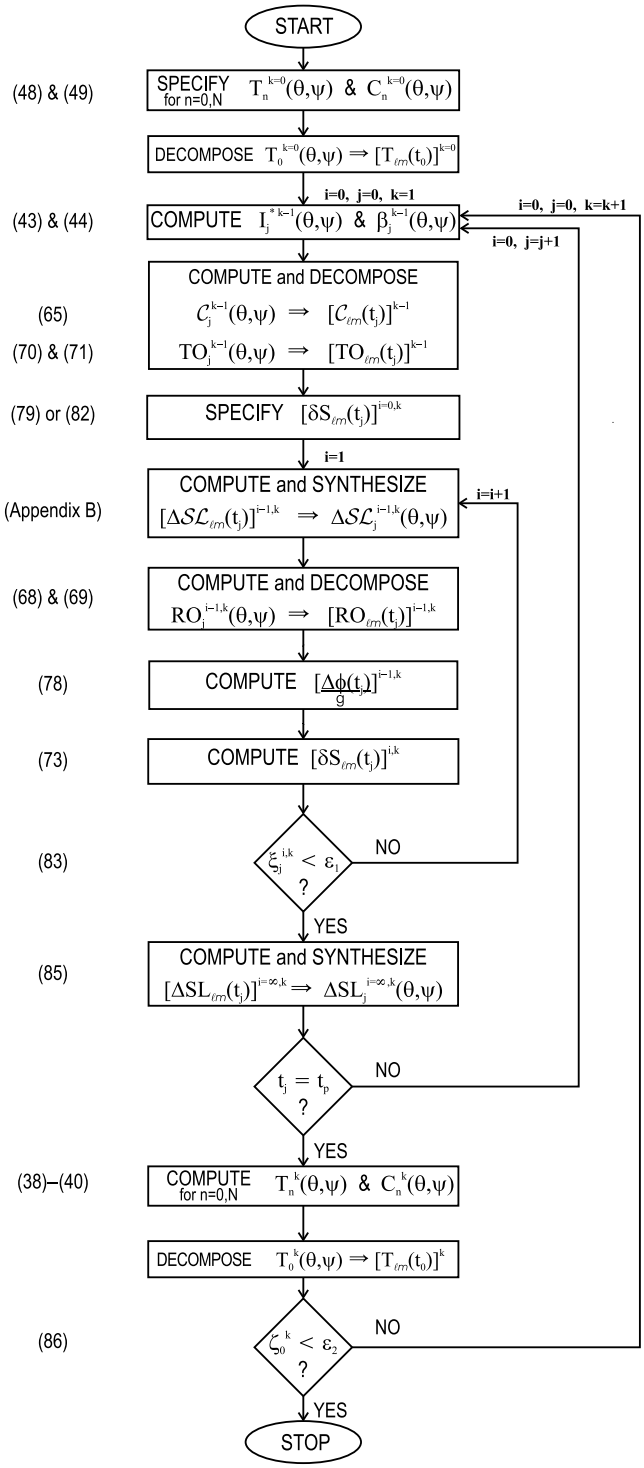

Figure 4. Flowchart outlining the algorithm for solving the sea-level equation on a spherically symmetric earth model with time-dependent continent margins. For a spherically symmetric viscoelastic earth model, $[\Delta\mathcal{SL}_{\ell m}(t_j)]^{i,k}$ can be computed using derivations in Appendix B: eq. (B18) for the case of a non-rotating earth and (B28) when rotation effects are included.

elsewhere (due either to marine transgression/regression or water influx into zones vacated by ablating grounded marine ice). In the remainder of this section, we explore this issue by attempting to isolate the signals associated with each of the processes in Fig. 1.

5.1 Effects of sea-level transgression and regression

To isolate the impact of shoreline evolution associated with transgression and regression, we begin by comparing predictions using the new and classic theories based on the DISK ice history (in this case, the no marine ice simplification in eq. 20 holds). The geographic variation

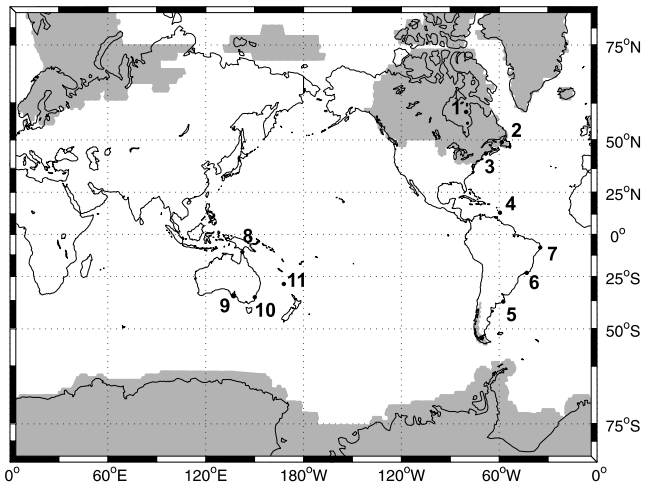

Figure 5. Map showing the extent of ice cover (shaded) at last glacial maximum according to the ICE-3G deglaciation history (Tushingham & Peltier 1991), as well as the location of various sites (1–11) referred to in the discussion of numerical results.

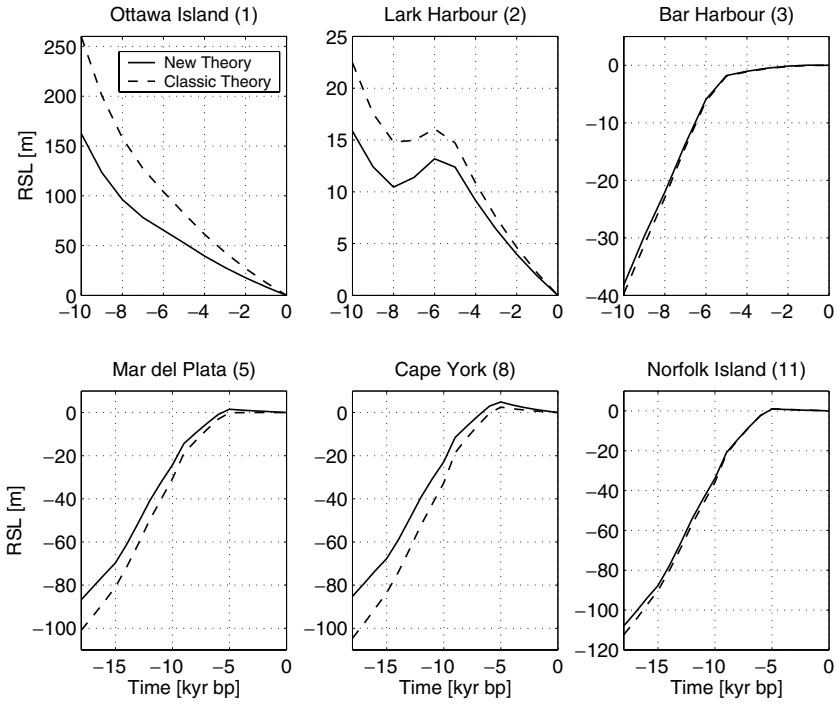

Figure 6. Predictions of relative sea-level change at six sites based on the new sea-level theory (solid line) and the classic, FC1976 sea-level equation (dashed line). The location of the sites is indicated (by site number) in Fig. 5. The predictions adopt an ice history modified from the ICE-3G model, as described in the text. The viscoelastic earth model is also specified in the text. Results for the new theory involve three iterations through the complete glacial cycle (i.e. $k = 3$); however, these predictions are not significantly altered beyond the second 'outer' iteration.

of the discrepancy in the two theories is evident in Fig. 7, where we plot maps of the difference in predicted relative sea level at LGM (18 kyr BP) and at the end of the deglaciation phase (5 kyr BP). As a companion to this figure, we also plot in Fig. 8 the complete post-LGM relative sea-level variation predicted using the new and classic theories at a set of six sites, three along the Australian coastline (left column), and three along the east coast of South America (see Fig. 5). The ordering of the sites in Fig. 8 is such that as one moves from top to bottom panel, the seaward steepness of the shelf increases (see Fig. 9).

The amplitude of the differential signal over both Australia and South America is strongly correlated with the local depth of the continental shelf, as has been noted in previous work (Lambeck & Nakada 1990; Milne & Mitrovica 1998b). The sign of the error in regions close to large shoreline evolution (i.e. shallow shelves) introduced by the FC1976 theory is relatively straightforward to understand. This classic theory assumes a cliff-like shoreline located at the present-day interface between land and continent. As deglaciation proceeds, and global ocean levels rise, this assumption overestimates the local ocean load which leads, in turn, to an overestimate of the local subsidence of the solid

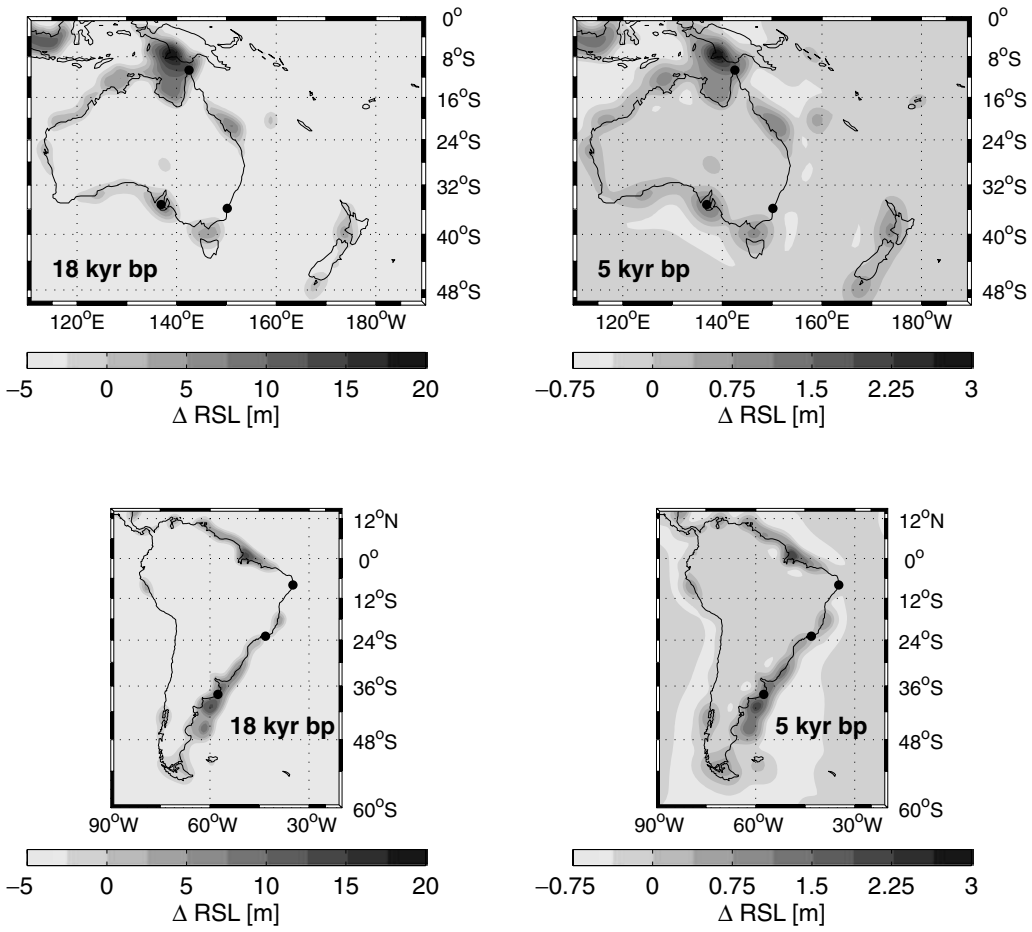

Figure 7. Maps showing the discrepancy in two predictions of relative sea-level change in the vicinity of Australia and South America at last glacial maximum (18 kyr BP) and at the end of the model deglaciation phase (5 kyr BP). The first prediction is based on the new sea-level theory while the second is generated using the classic, FC1976 sea-level equation (plots show 'new' minus 'classic'). The calculations adopt the DISK ice history and the viscoelastic earth model specified in the text. The former was constructed to exclude any marine-based component.

surface. Following eq. (1), the net result is an overestimate by the classic sea-level theory of the post-LGM sea-level rise at sites such as Cape York in northern Australia and Mar del Plata in southeast South America by 10–20 m.

It is interesting to note that the sign of the discrepancy reverses for sites such as Moruya and Recife, which are located in the vicinity of a relatively steep shelf (Fig. 8). The reason for this is connected to the integrated impact of incorporating shelf topography into the sea-level predictions. Since the new sea-level theory accounts for shelf topography seaward of present-day shorelines, a given volume of meltwater will raise global mean sea level more than a calculation which assumes that all shorelines are steep vertical cliffs. Thus, the discrepancy (new minus classic) at any site away from ocean loading effects associated with shoreline evolution, including the open ocean areas in Fig. 7, will be negative. The left frames in Fig. 7 are characterized by a value of $\sim$2 m in such zones, indicating that the post-LGM eustatic sea-level rise is underestimated by about 2 per cent in calculations where one simply divides the net meltwater volume by the present-day area of the oceans.

We next turn our attention to an assessment of the error incurred in previous efforts to incorporate transgression/regression at shorelines into the traditional sea-level theory (Fig. 1a). Analytic expressions defining these previous efforts were summarized in Section 2.2.1.

The approaches described by Johnston (1993) (see also Lambeck & Nakada 1990) and by Milne & Mitrovica (1998b) (see also Milne 1998; Milne *et al.* 1999), given by eqs (26) and (29), respectively, are based on approximations to the change in the ocean load over individual time increments in the sea-level solution (e.g. from t_{j-1} to t_j). Specifically, the ocean load increment is approximated as the change in global sea level during the time increment projected on to some representative ocean function. The two approaches differ only in the choice of this ocean function. Johnston (1993) adopted an ocean function consistent with the shoreline position at some intermediate stage within the time increment (eq. 26), while Milne (1998) used the ocean function at the end of the time increment (eq. 29). The error associated with the Johnston (1993) algorithm will be dependent on the precise choice for the 'representative' ocean function but we have found, in numerical tests, that this error is nearly identical in amplitude and geometry to the error incurred using the Milne (1998) approximation, and so we focus on the latter here.

Eq. (30) indicates that, within each time step, the error in the ocean load introduced by the Milne (1998) algorithm is equal to the topography at the beginning of the time step, $T(\theta, \psi, t_{j-1})$, within the zone of shoreline evolution from t_{j-1} to t_j (i.e. the geographic region

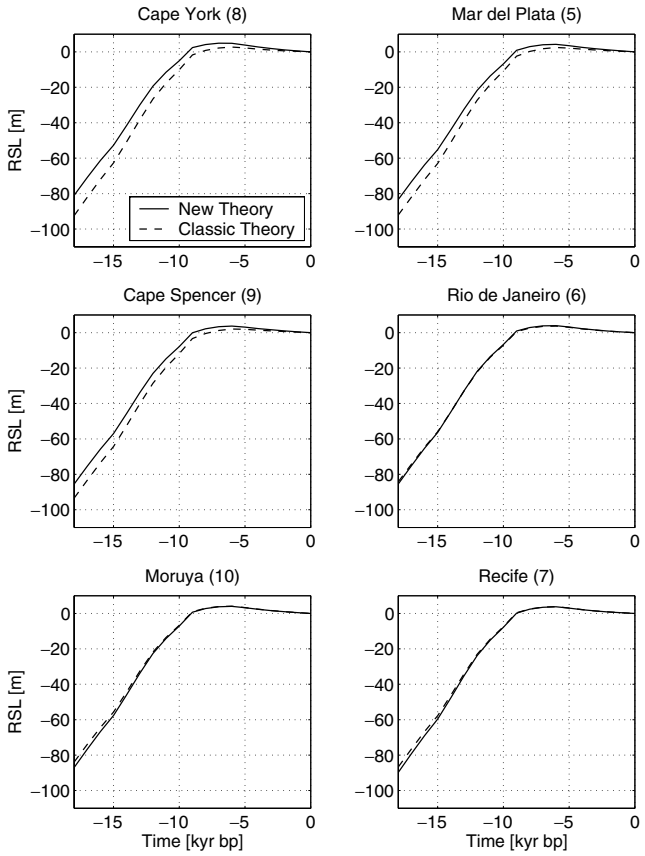

Figure 8. Predictions of relative sea-level change at six sites based on the new sea-level theory (solid line) and the classic, FC1976 sea-level equation (dashed line). The location of the sites is indicated (by site number) in Fig. 5. The predictions adopt the DISK ice history and the viscoelastic earth model described in the text.

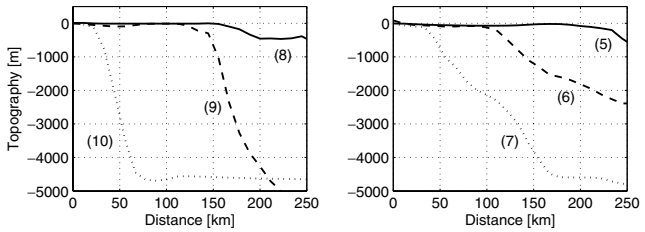

Figure 9. The topography of the solid Earth as a function of distance seaward of the six sites considered in Fig. 8. The location of these sites is indicated (by site number) in Fig. 5.

in which $C(\theta, \psi, t_j)$ and $C(\theta, \psi, t_{j-1})$ differ). Fig. 7 of Paper I provides a schematic illustration of the accumulated error eight steps into a model deglaciation phase. Clearly, the steeper the local shoreline geometry, or the smaller the time increments, the less the error incurred by the Milne (1998) approach. Indeed, we have found that the magnitude of the error decreases significantly when the time steps are halved.

In Fig. 10 we show differences in predictions generated using the new sea-level theory and the Milne (1998) formulation. This figure can be directly compared to Fig. 7, which showed the analogous error introduced by the FC1976 sea-level formulation. As expected, the discrepancies evident in Fig. 10 are largest in regions with significant shoreline evolution in the post-LGM period. However, the error in these regions is reduced by a factor of ∼10 relative to predictions based on the FC1976 theory. One example is the Arafura Sea between Australia and New Guinea; the post-LGM sea-level rise predicted using the FC1976 theory has a maximum error of ∼15 m, or 15 per cent of the total (order 100 m) sea-level rise, while the Milne (1998) algorithm reduces this error to just 1.5 m or ∼1.5 per cent. Note also that the error in regions with steep shorelines or over the open ocean is close to zero in Fig. 10, in contrast to results in Fig. 7, indicating that the Milne (1998) algorithm accurately captures the integrated impact of shoreline topography on eustatic sea-level change.

In Fig. 11 we investigate the accuracy of the Peltier (1994) theory for treating shoreline evolution in the absence of marine-based ice. According to eq. (27), this approach is based on an approximation to the ocean load from the onset of loading, rather than across a single time increment, and the error in the load introduced at some time t_j is equal to the topography at t_0 within the zone of shoreline evolution from t_0 to t_j (eq. 28). A schematic illustration of this error, for a loading history beginning at LGM, was given in fig. 6 of Paper I; this schematic

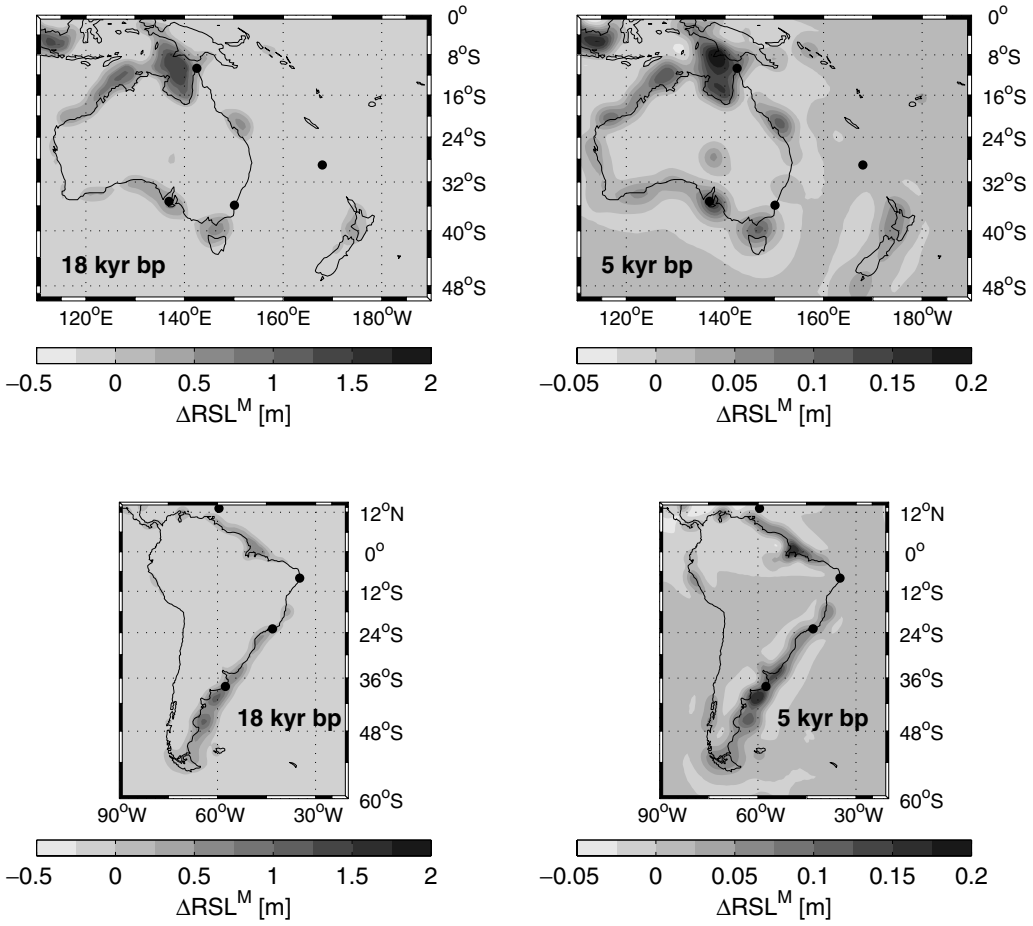

Figure 10. Maps showing the discrepancy in two predictions of relative sea-level change in the vicinity of Australia and South America at last glacial maximum (18 kyr BP) and at the end of the model deglaciation phase (5 kyr BP). The first prediction is based on the new sea-level theory while the second is generated using the sea-level theory derived by Milne (1998) (see eqs 29 and 30) (plots show 'new' minus approximate). The calculations adopt the DISK ice history and the viscoelastic earth model specified in the text. The former was constructed to exclude any marine-based component.

suggests a large accumulated error in the ocean load which reaches an amplitude of order 100 m in zones of shoreline migration, irrespective of the size of the time increments. In Paper I we suggested, on the basis of these arguments, that predictions of relative sea-level histories based on the Peltier (1994) approach would, in regions of shoreline evolution, be subject to large errors. This qualitative assertion is supported by the numerical results in Fig. 11, which indicate that the peak error incurred by the approach defined in eq. (27) is of amplitude comparable to the error associated with the traditional FC1976 sea-level algorithm (compare Figs 11 and 7). We have found that the magnitude of the error associated with the Peltier (1994) approach does not significantly decrease when the time steps are halved. The schematic provided in Paper I demonstrates that the Peltier (1994) approach will overestimate the ocean load, and thus the load-induced subsidence, in regions of shoreline evolution during deglaciation. Hence, the post-LGM sea-level rise predicted using the approach will be larger than it should be, and this explains the sign of the error evident in Fig. 11.

Peltier & Drummond (2002) have recently described the inclusion of a 'broad-shelf effect' as an improvement to the Peltier (1994) treatment of shoreline migration associated with local transgression and regression. Since no mathematical details are provided in Peltier & Drummond (2002), we cannot robustly assess the nature of this improvement, though they do appear to recognize that the ocean load generated by the Peltier (1994) approximation does not 'conform to the volume bounded by the local paleotopography' (p. 10–2). Their analysis, which focused on predictions along the east coast of South America, yields a 'broad-shelf' correction consistent with the amplitude of the error evident in Fig. 11. In any case, it is clear from the results in Fig. 10 that the broad-shelf effect introduced by Peltier & Drummond (2002) is already included in earlier algorithms that treated shoreline migration (e.g. Lambeck & Nakada 1990; Johnston 1993; Milne 1998; Milne & Mitrovica 1998b; Milne *et al.* 1999).

In Fig. 12 we revisit RSL predictions at the six sites in Fig. 8. In particular, the solid lines in Fig. 12 represent the discrepancy between the new and classic predictions in Fig. 8. For the purpose of comparison the dashed and dotted lines in Fig. 12 are analogous errors incurred when the Milne (1998) and Peltier (1994) algorithms are adopted, respectively, to treat the shoreline migration processes in Fig. 1(a). The error associated with the Milne (1998) algorithm (and thus also the Nakada & Lambeck 1989; Johnston 1993, approaches) are negligible at each site; in contrast, the error associated with the Peltier (1994) procedure is comparable to the error in the classic FC1976 theory.

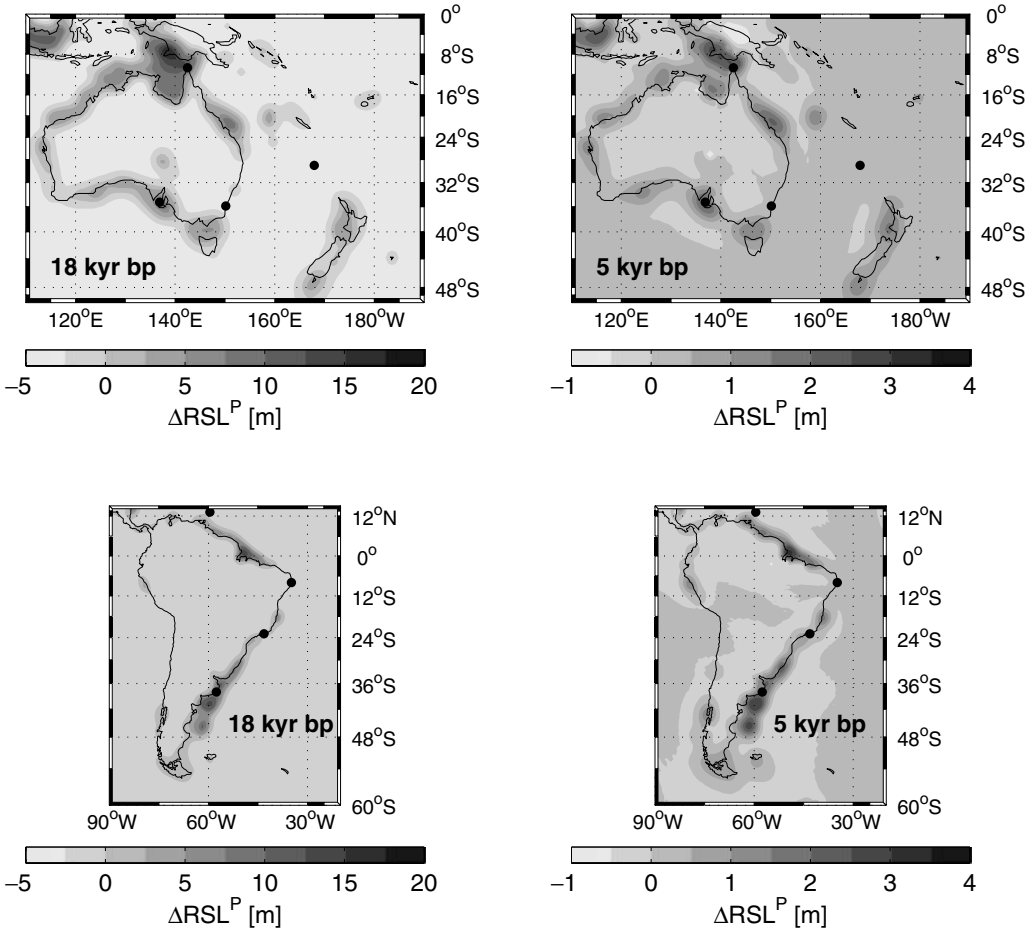

Figure 11. Maps showing the discrepancy in two predictions of relative sea-level change in the vicinity of Australia and South America at last glacial maximum (18 kyr BP) and at the end of the model deglaciation phase (5 kyr BP). The first prediction is based on the new sea-level theory while the second is generated using the sea-level theory derived by Peltier (1994) (see eqs 27 and 28) (plots show 'new' minus approximate). The calculations adopt the DISK ice history and the viscoelastic earth model specified in the text. The former was constructed to exclude any marine-based component. To be consistent with the analysis of Peltier (1994), we use a form of the DISK ice history which assumes initial isostatic equilibrium at LGM.

5.2 Effects due to changes in marine-based ice

We next consider the issue of local and far-field sea-level changes driven by water inundation into zones of ablating, marine-based ice (as in Fig. 1) or water displacement during the growth of such ice complexes. In this case, we return to the ICE-3G ice history and we begin by comparing two predictions. The first is based on the new sea-level theory; specifically, the extended pseudo-spectral formulations in Section 4.2 coupled with Appendix B1. The second involves the same set of equations with the exception that no account is taken for marine-based ice (henceforth the 'standard' solution). In practice, the latter predictions are generated by replacing the field C^k (see eq. 65) which appears in the governing equations (e.g. 66) by C^k; that is, we assume that while marine-based ice complexes load the planet, they do not influence the ocean accommodation space for meltwater. This assumption is consistent with earlier sea-level algorithms (e.g. Farrell & Clark 1976; Mitrovica & Peltier 1991; Johnston 1993; Peltier 1994) in which all ice sheets were implicitly treated as land-based. Furthermore, any discrepancies between the two predictions will arise solely from the impact of the process in Fig. 1(b), since the shoreline migration process in Fig. 1(a) is accurately incorporated into both.

Fig. 13 shows the difference in relative sea-level change within eastern North America over the last 9, 7, and 5 kyr, predicted on the basis of the new and standard approaches. The Hudson Bay region was covered by a large marine-based ice complex at LGM that rapidly collapsed ∼10 kyr BP in the ICE-3G model; the same ice history also includes marine-based ice cover on the east coast of Canada between Newfoundland and the mainland at LGM (Fig. 5). As a companion to these maps, Fig. 14 shows relative sea-level histories at four sites predicted using the new and standard algorithms (solid and dashed lines, respectively).

It is clear that the water inundation process in Fig. 1(b) has a profound impact on predictions of relative sea-level change in the vicinity of ancient marine-based ice complexes (Milne 1998; Milne *et al.* 1999). Within Hudson Bay, the error incurred by adopting a sea-level theory which neglects this physics exceeds 100 m for beaches formed just after the collapse of the ice sheet. In this regard, the inundation of water into the region vacated by marine ice will act to retard the post-glacial uplift of the region and hence the post-glacial sea-level rise predicted using the new theory will be smaller than that generated from the standard approach (note the sign of the discrepancy in Fig. 13 and the results

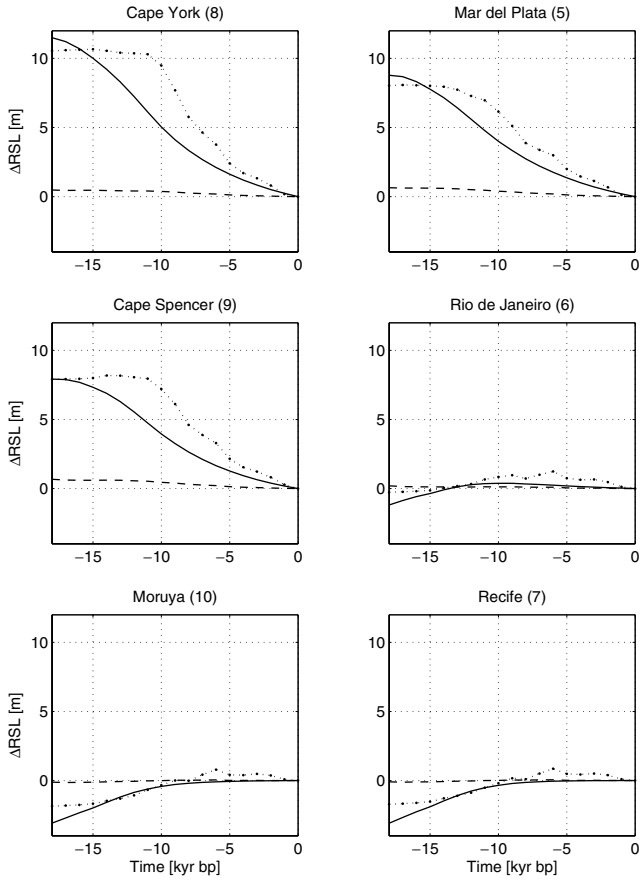

Figure 12. Comparing the accuracy of predictions of relative sea-level change at the same six sites considered in Fig. 8. Each line refers to the discrepancy between a prediction based on the new sea-level theory and predictions generated using the classic theory (solid line), the Milne approximation (dashed line) and the Peltier approximation (dotted line) (plots show 'new' minus approximate). The calculations adopt the DISK ice history and the viscoelastic earth model specified in the text. To be consistent with Peltier (1994), the dotted line predictions use a form of the DISK ice history which assumes initial isostatic equilibrium at LGM.

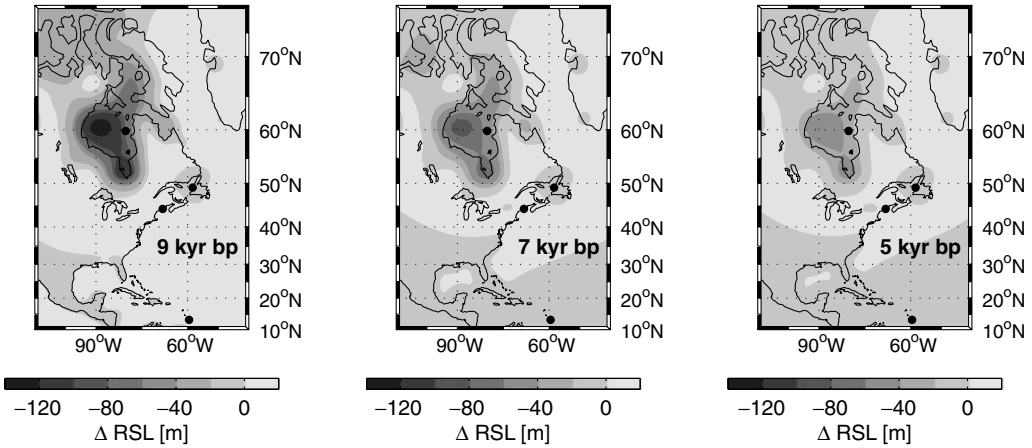

Figure 13. Maps showing the discrepancy in two predictions of relative sea-level change in the vicinity of eastern North America at 9, 7, and 5 kyr BP. The first prediction is based on the new sea-level theory while the second is generated using the same theory with the exception that no account is taken of the shoreline migration associated with variations in marine-based ice ('standard' theory; see eq. 65 and text for details). (Plots show 'new' minus standard.) The calculations adopt the modified ICE-3G ice history and the viscoelastic earth model specified in the text.

for the Ottawa Island site in Fig. 14). A comparison of predictions for Ottawa Island and Lark Harbour in Figs 6 and 14 indicates that the discrepancy we originally noted between the new and classic sea-level theories (where the latter includes no shoreline migration processes of any kind) was due almost entirely to the treatment of marine-based ice. In contrast, the discrepancy at Bar Harbor in Fig. 6, located near the perimeter of the Laurentian ice complex at LGM, has contributions from both shoreline migration processes illustrated in Fig. 1.

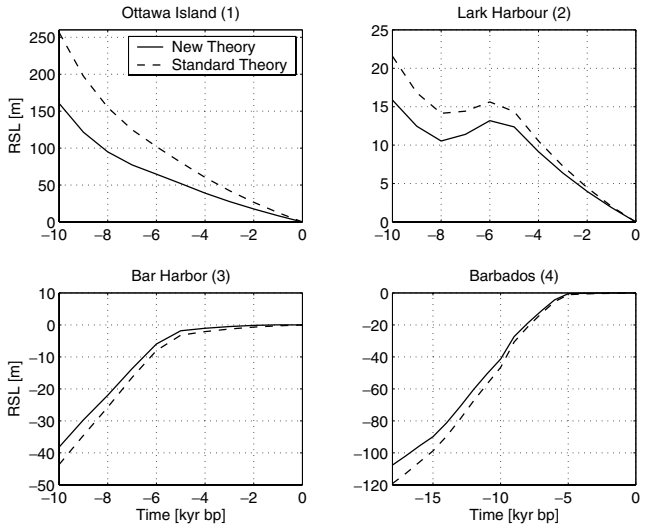

Figure 14. Predictions of relative sea-level change at four sites based on the new sea-level theory (solid) and the standard theory (dashed) described in the text which is modified from the new theory so that no account is taken of shoreline migration associated with variations in marine-based ice. The location of the sites is indicated (by site number) in Fig. 5. The predictions adopt the modified ICE-3G ice history and the viscoelastic earth model specified in the text.

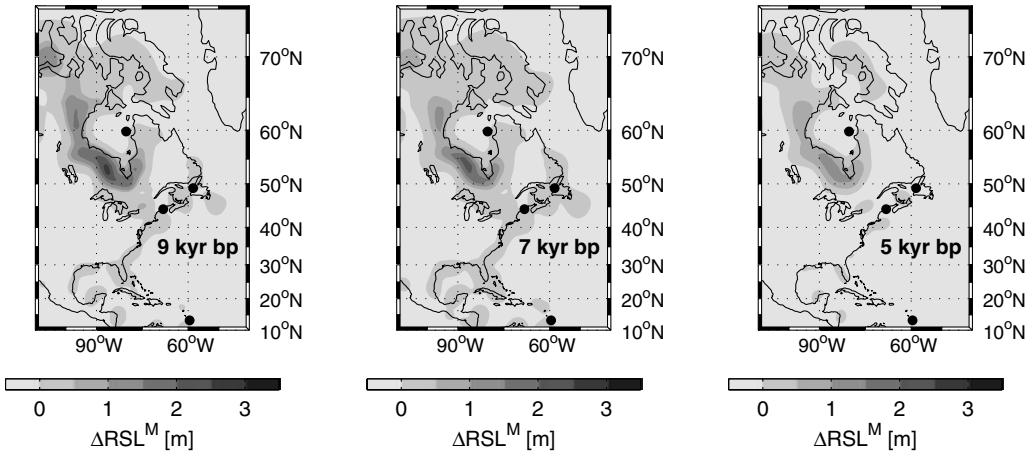

Figure 15. Maps showing the discrepancy in two predictions of relative sea-level change in the vicinity of eastern North America at 9, 7, and 5 kyr BP. The first prediction is based on the new sea-level theory while the second is generated using the sea-level equation derived by Milne (1998) and Milne *et al.* (1999) (eqs 31 and 32). (Plots show 'new' minus approximate.) The calculations adopt the modified ICE-3G ice history and the viscoelastic earth model specified in the text.

The final site in Fig. 14, Barbados, is at the far-field of any late Pleistocene ice complex and thus the discrepancy associated with the new and standard sea-level algorithms at this site is a measure of the integrated accommodation space produced by melting ice during the last deglaciation phase, i.e. the net space in 'holes' left by the retreating marine-ice complexes. Since this discrepancy exceeds 10 m, it is clear that the inaccurate treatment of shoreline migration in the vicinity of marine-based ice sheets may introduce significant (order 10 per cent) error in the inference of excess ice volumes based on far field sea-level records (Milne 1998; Peltier 1998b; Milne *et al.* 1999).

As discussed in the Introduction, two approaches have been described for incorporating the shoreline migration process in Fig. 1(b) into predictions of post-glacial sea-level change. The first, by Milne (1998) (see also Milne *et al.* 1999), who coined the term 'water dumping', was based on a revised version of the classic FC1976 sea-level equation (31) which attempted to incorporate the gravitational and loading effects of the influx. The error in the ocean load introduced by this approach (relative to the exact expressions upon which our new theory is based) is given by the second term on the RHS of eq. (32). A second approach, by Peltier (1998b), involved no revision to the sea-level theory; rather, he used the theory outlined in Peltier (1994) and performed an *a posteriori* calculation of the total volume of the holes left behind by ablating marine ice complexes. Peltier (1998b) adopted this volume, which was the dominant contributor to an 'implicit ice field', to improve estimates of eustatic sea-level change associated with each of the major late Pleistocene ice complexes. Since the water inundation is not explicitly treated within the Peltier (1998b) sea-level theory, the gravitational and loading effects on site-specific relative sea-level histories do not appear to be included. It is clear from the results at Ottawa Island and Lark Harbour in Fig. 14 that such effects can be significant.

To complete this section, we assess the accuracy of the Milne (1998) approach to treating marine-based ice. Specifically, Fig. 15 is analogous to Fig. 13, with the exception that we plot the discrepancy between predictions based on our new sea-level theory and those

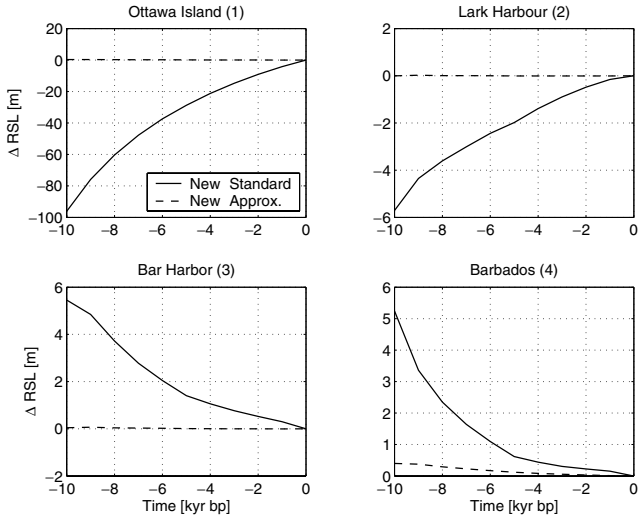

Figure 16. Comparing the discrepancies between two predictions of relative sea-level change at the same four sites illustrated in Fig. 14. The first prediction is based on the new sea-level theory while the second is generated using the standard theory (solid line) and the Milne approximation (dashed line) (plots show 'new' minus approximate). The calculations adopt the modified ICE-3G ice history and the viscoelastic earth model specified in the text.

generated by adopting eq. (32). This error is geographically localized within the zone of shoreline migration surrounding Hudson Bay. This pattern indicates that the discrepancy arises predominantly from the Milne (1998) treatment of the transgression/regression process in Fig. 1(a) (which we investigated in the last section), rather than from errors associated with the modelling of marine-based ice flux. In any event, this discrepancy is small, and negligible in relation to the error incurred using the standard theory (Fig. 13). To reinforce this point, Fig. 16 compares errors in the prediction of RSL histories associated with the standard theory (solid line; difference between the solid and dashed lines in Fig. 14) and the water influx algorithm of Milne (1998). Clearly, the Milne (1998) procedure yields a very accurate approximation to our generalized sea-level theory.

6 SUMMARY

At the most basic level, a theory of post-glacial sea-level change requires two inputs. The first is a mapping between variations in global sea level and changes in ocean height (or ocean load). The second is a theoretical or numerical methodology for computing global sea-level variations given an arbitrary surface load. In the classic sea-level theory of FC1976, an assumption of fixed shoreline location is made and the first of these elements is then trivially expressed as a projection of the global sea-level variation on to the present-day ocean function. In Paper I of this series we derived exact expressions for the mapping in the case of shoreline migration due to either of the processes in Fig. 1. These expressions are valid for any earth model, but they are not in a form amenable to numerical solution.

In Section 3 of this paper we provided an efficient, iterative numerical algorithm for solving the exact, generalized sea-level theory outlined in Paper I. The algorithm requires two nested iterations. The first, 'inner' iteration acts within a single time step in the sea-level solution, and involves the successive improvement of a first guess to the ocean height change within the time increment. This iteration reflects the well known integral nature of the sea-level equation; specifically, though global sea-level variations define ocean load changes, they are also influenced by these changes. The second, 'outer' iteration is performed over the complete loading history, and it involves the successive improvement of an estimate of the initial (prior to onset of loading) topography field. Our detailed description of the numerical algorithm provided a set of reasonable 'first guesses' to all quantities subject to iterative refinement.

The vast majority of GIA analyses have focused (and continue to focus) on spherically symmetric earth models. In Section 4 we provided a special case of our generalized theory that is valid for such models. The algorithm makes use of viscoelastic Love number theory for computing the response to an arbitrary surface load, and it represents an extension of the commonly adopted pseudo-spectral algorithm derived by Mitrovica & Peltier (1991) for the fixed-shoreline case.

We adopted the non-rotating form of this algorithm in Section 5. In particular, we quantitatively assessed the accuracy of previous (approximate) procedures developed to extend the fixed-shoreline theory of FC1976 to treat the processes shown in Fig. 1. These previous efforts, all implemented on spherically symmetric earth models, have been subject to debate (see Mitrovica 2003, for a review). Our conclusions within this section support qualitative arguments that appeared in Paper I. Namely, ocean loading effects associated with transgression/regression cycles at shallow shorelines are accurately captured (to order 1 per cent error) by procedures described in Lambeck & Nakada (1990), Johnston (1993), Milne (1998), Milne & Mitrovica (1998a) and Milne *et al.* (1999). In contrast, the error incurred by the algorithm of Peltier (1994) is an order of magnitude higher. In this respect, the 'broad-shelf effect' recently introduced by Peltier & Drummond (2002) appears to be a correction to address this larger error term. We also conclude that the Milne (1998) treatment of marine-based ice accurately captures the

impact of the water inundation process shown in Fig. 1(b). In contrast, while the *a posteriori* 'implicit ice' calculation applied by Peltier (1998b) approximates the impact of the process on estimates of eustatic sea-level change, it does not appear to incorporate the large local loading effects associated with the water inundation.

In the third and final paper in this series we couple our generalized sea-level methodology with a finite-element numerical procedure to compute gravitationally self-consistent post-glacial sea-level change on earth models with 3-D variations in viscoelastic structure. We verify that the conclusions in Section 5, regarding the potential importance of the shoreline migration processes in Fig. 1, are unaltered by the move to more complex earth models. Hence, our focus in future work will be to analyse the sensitivity of sea-level predictions, at sites in the near-, mid-, and far-field of the Pleistocene ice sheets, to variations in lithospheric thickness and mantle viscosity.

ACKNOWLEDGMENTS

This work was supported by an OGSST scholarship (to RK), an NSERC Research Grant (to JXM), the Canadian Institute for Advanced Research and the Miller Institute for Basic Sciences.

REFERENCES

Bills, B.G. & James, T.S., 1996. Late Quaternary variations in relative sea level due to glacial cycle polar wander, *Geophys. Res. Lett.,* **23,** 3023–3026.

Clark, J.A., Farrell, W.E. & Peltier, W.R., 1978. Global changes in postglacial sea level: A numerical calculation, *Quat. Res.,* **9,** 265–287.

Dahlen, F.A., 1976. The passive influence of the oceans upon the rotation of the Earth, *Geophys. J. R. astr. Soc.,* **46,** 363–406.

Dziewonski, A.M. & Anderson, D.L., 1981. Preliminary reference Earth model (PREM), *Phys. Earth planet. Inter.,* **25,** 297–356.

Farrell, W.E. & Clark, J.A., 1976. On postglacial sea level, *Geophys. J. R. astr. Soc.,* **46,** 647–667.

Giunchi, C. & Spada, G., 2000. Postglacial rebound in a non-Newtonian spherical Earth, *Geophys. Res. Lett.,* **27,** 2065–2068.

Han, D. & Wahr, J., 1989. Post-glacial rebound analysis for a rotating Earth, in *Slow Deformations and Transmission of Stress in the Earth,* pp 1–6, eds Cohen, S. & Vanicek, P., AGU Mono. Series 49.

Johnston, P., 1993. The effect of spatially non-uniform water loads on predictions of sea level change, *Geophys. J. Int.,* **114,** 615–634.

Lambeck, K. & Nakada, M., 1990. Late Pleistocene and Holocene sea level change along the Australian coast, *Palaeogeog. Palaeoclimat. Palaeoecol.,* **89,** 143–176.

Lambeck, K., Smither, C. & Johnston, P., 1998. Sea level change, glacial rebound and mantle viscosity for northern Europe, *Geophys. J. Int.,* **134,** 102–144.

Lambeck, K., Purcell, A., Johnston, P., Nakada, M. & Yokoyama, Y., 2003. Water-load definition in the glacio-hydro-isostatic sea level equation, *Quat. Sci. Rev.,* **22,** 309–318.

Latychev, K., Mitrovica, J.X., Tromp, J., Tamisiea, M.E., Komatitsch, D. & Christara, C., 2005. Glacial isostatic adjustment on 3-D Earth models: a finite-volume formulation, *Geophys. J. Int.,* **161,** 421–444.

Martinec, Z., 2000. Spectral-finite element approach to three-dimensional viscoelastic relaxation in a spherical earth, *Geophys. J. Int.,* **142,** 117–141.

Milne, G.A., 1998. Refining models of the glacial isostatic adjustment process, *PhD thesis,* University of Toronto, Toronto.

Milne, G.A., 2002. Recent advances in predicting glaciation-induced sea-level changes and their impact on model applications, in *Ice sheets, sea level and the dynamic Earth,* pp 157–176, eds. Mitrovica, J.X. & Vermeersen, B.L A., AGU Geodynamics Series 29.

Milne, G.A & Mitrovica, J.X., 1996. Postglacial sea-level change on a rotating Earth: First results from a gravitationally self-consistent sea-level equation, *Geophys. J. Int.,* **126,** F13–F20.

Milne, G.A. & Mitrovica, J.X., 1998a. Postglacial sea level change on a rotating Earth, *Geophys. J. Int.,* **133,** 1–10.

Milne, G.A. & Mitrovica, J.X., 1998b. The influence of time-dependent ocean-continent geometry on predictions of post-glacial sea level change in Australia and New Zealand, *Geophys. Res. Lett.,* **25,** 793–796.

Milne, G.A., Mitrovica, J.X. & Davis, J.L., 1999. Near-field hydro-isostasy: The implementation of a revised sea-level equation, *Geophys. J. Int.,* **139,** 464–482.

Milne, G.A., Mitrovica, J.X. & Schrag, D.P., 2001. Estimating past continental ice volumes from sea-level data, *Quat. Sci. Rev.,* **21,** 361–376.

Mitrovica, J.X., 2003. Recent controversies in predicting post-glacial sea-level change: A viewpoint, *Quat. Sci. Rev.,* **22,** 127–133.

Mitrovica, J.X. & Peltier, W.R., 1989. Pleistocene deglaciation and the global gravity field, *J. geophys. Res.,* **94,** 13 651–13 671.

Mitrovica, J.X. & Peltier, W.R., 1991. On postglacial geoid subsidence over the equatorial oceans, *J. geophys. Res.,* **96,** 20 053–20 071.

Mitrovica, J.X. & Milne, G.A., 2003. On post-glacial sea level: I. General theory, *Geophys. J. Int.,* **154,** 253–267.

Mitrovica, J.X., Milne, G.A. & Davis, J.L., 2001. Glacial isostatic adjustment on a rotating Earth, *Geophys. J. Int.,* **147,** 562–579.

Mitrovica, J.X., Wahr, J., Matsuyama, I. & Paulson, A., 2005. The rotational stability of an ice-age earth, *Geophys. J. Int.,* **161,** 491–506.

Munk, W.H. & MacDonald, G.J.F., 1960. *The rotation of the Earth,* Cambridge Univ. Press, New York.

Nakada, M. & Lambeck, K., 1989. Late Pleistocene and Holocene sea-level change in the Australian region and mantle rheology, *Geophys. J. Int.,* **96,** 497–517.

Peltier, W.R., 1974. The impulse response of a Maxwell Earth, *Rev. Geophys.,* **12,** 649–669.

Peltier, W.R., 1976. Glacial isostatic adjustment, 2, The inverse problem, *Geophys. J. R. astr. Soc.,* **46,** 669–706.

Peltier, W.R., 1994. Ice age paleotopography, *Science,* **265,** 195–201.

Peltier, W.R., 1998a. Postglacial variations in the level of the sea: Implications for climate dynamics and solid-Earth geophysics, *Rev. Geophys.,* **36,** 603–689.

Peltier, W.R., 1998b. 'Implicit ice' in the global theory of glacial isostatic adjustment, *Geophys. Res. Lett.,* **25,** 3955–3958.

Peltier, W.R. & Andrews, J.T., 1976. Glacial-isostatic adjustment I – the forward problem, *Geophys. J. R. astr. Soc.,* **46,** 605–646.

Peltier, W.R. & Drummond, R., 2002. A 'broad-shelf effect' upon post-glacial relative sea level history, *Geophys. Res. Lett.,* **29,** 10.1029/2001GL014273.

Tromp, J. & Mitrovica, J.X., 1999. Surface loading of a viscoelastic Earth - I. General theory, *Geophys. J. Int.,* **137,** 847–855.

Tushingham, A.M. & Peltier, W.R., 1991. ICE-3G: A new global model of late Pleistocene deglaciation based on geophysical predictions of post-glacial relative sea level change, *J. geophys. Res.,* **96,** 4497–4523.

Wu, P. & Peltier, W.R., 1983. Glacial isostatic adjustment and the free air gravity anomaly as a constraint on deep mantle viscosity, *Geophys. J. R. astr. Soc.,* **74,** 377–449.

Wu, P. & van der Wal, W., 2003. Postglacial sealevels on a spherical, self-gravitating viscoelastic Earth: effects of lateral viscosity variations in the upper-mantle on the inference of viscosity contrasts in the lower mantle, *Earth. planet. Sci. Lett.,* **211,** 57–68.

Zhong, S., Paulson, A. & Wahr, J., 2003. Three-dimensional finite-element modelling of Earth's viscoelastic deformation: effects of lateral variations in lithospheric thickness, *Geophys. J. Int.,* **155,** 679–695.

APPENDIX A: A NUMERICAL ALGORITHM FOR SOLVING THE GSLE: SPECIAL CASES

In Section 3 we developed an iterative numerical algorithm for solving the generalized sea-level equation (19). In this appendix we provide the analogous iteration equations for the special cases where there are no marine-based ice complexes, and, additionally, where the continent margins remain fixed with time. The sea-level equations governing these two special cases are given by (22) and (25), respectively.

A1 No marine ice

When there is no marine ice, $I^*(\theta, \psi, t_j) = I(\theta, \psi, t_j)$ and $C(\theta, \psi, t_j)\, \beta(\theta, \psi, t_j) \Rightarrow C(\theta, \psi, t_j)$. Rewriting (45) and dropping the $k-$iteration counter on the ice load, the equation to be solved is

$$\delta S_j^{i,k} = -\Delta S_{j-1}^{i=\infty,k} + \Delta \mathcal{SL}_j^{i-1,k} \left({}^{\delta I_m}_{0\le m\le j};{}^{\delta S_m^{i=\infty,k}}_{0\le m<j};\delta S_j^{i-1,k} \right) C_j^{k-1} + \frac{\Delta\Phi_j^{i-1,k}}{g} C_j^{k-1} - T_0^{k-1}\left[C_j^{k-1} - C_0^{k-1}\right]. \tag{A1}$$

Furthermore, we update (46) to

$$\frac{\Delta\Phi_j^{i-1,k}}{g} = -\frac{1}{A_j^{k-1}}\frac{\rho_{\rm i}}{\rho_{\rm w}} \iint_\Omega \Delta I_j d\Omega - \frac{1}{A_j^{k-1}} \iint_\Omega \Delta \mathcal{SL}_j^{i-1,k} \left({}^{\delta I_m}_{0\le m\le j};{}^{\delta S_m^{i=\infty,k}}_{0\le m<j};\delta S_j^{i-1,k} \right) C_j^{k-1} d\Omega + \frac{1}{A_j^{k-1}} \iint_\Omega T_0^{k-1}\left[C_j^{k-1} - C_0^{k-1}\right] d\Omega, \tag{A2}$$

where

$$A_j^{k-1} = \iint_\Omega C_j^{k-1} d\Omega \tag{A3}$$

is the area of the oceans at time t_j.

There is no change from the general case in the calculation of the kth iterate topography fields and ocean functions. That is, T_0^k, T_j^k and C_j^k are calculated using (38)–(40).

A1.1 First guess $k = 0$

If, as in the general case, we let the $k = 0$ first guess topography field at each time t_j be equivalent to the present-day topography, then the ocean functions at each time t_j will all be equal to the present-day ocean function. The sea-level iteration algorithm (A1) then reduces to

$$\delta S_j^{i,k=1} = -\Delta S_{j-1}^{i=\infty,k=1} + \Delta \mathcal{SL}_j^{i-1,k=1} \left({}^{\delta I_m}_{0\le m\le j};{}^{\delta S_m^{i=\infty,k=1}}_{0\le m<j};\delta S_j^{i-1,k=1} \right) C_p + \frac{\Delta\Phi_j^{i-1,k=1}}{g} C_p. \tag{A4}$$

Furthermore, (A2) reduces to

$$\frac{\Delta\Phi_j^{i-1,k=1}}{g} = -\frac{1}{A_p}\frac{\rho_{\rm i}}{\rho_{\rm w}} \iint_\Omega \Delta I_j d\Omega - \frac{1}{A_p} \iint_\Omega \Delta \mathcal{SL}_j^{i-1,k=1} \left({}^{\delta I_m}_{0\le m\le j};{}^{\delta S_m^{i=\infty,k=1}}_{0\le m<j};\delta S_j^{i-1,k=1} \right) C_p\, d\Omega, \tag{A5}$$

where

$$A_p = \iint_\Omega C_p\, d\Omega \tag{A6}$$

is the area of the present-day oceans. Eqs (A4)–(A6) could also have been derived from (53)–(55) in the special case of no marine ice.

A1.2 First guess $i = 0$

To start each i-loop, we again require a first guess, $\delta S_j^{i=0,k}$. For the fixed margins case of $k = 1$, this is the purely eustatic rise illustrated in Fig. 3(a). As before, we use conservation of mass and find that the eustatic first guess is given by

$$\delta S_j^{i=0,k=1} = -\frac{\rho_{\rm i}}{\rho_{\rm w}}\frac{C_p}{A_p} \iint_\Omega \delta I_j\, d\Omega, \tag{A7}$$

where now the uniform change in ocean height occurs over the full area of the present-day oceans. Eq. (A7) follows from (58) in the special case of no marine ice. For the $k > 1$ iterations through the glacial cycle, we use the change in ocean height determined in the previous glacial cycle as first guess, as given by (59).

A2 Fixed continent margins and no marine ice

Again, in the absence of marine ice, $I^*(\theta, \psi, t_j) = I(\theta, \psi, t_j)$ and $C(\theta, \psi, t_j)\ \beta(\theta, \psi, t_j) \Rightarrow C(\theta, \psi, t_j)$. Furthermore, for time independent continent margins, represented by the steep vertical cliffs at all shorelines adopted in the classic treatment of post-glacial sea-level change, we have $C(\theta, \psi, t_j) = C(\theta, \psi)$ for all times t_j. In this case, the known present-day ocean function $C_p(\theta, \psi)$ is adopted, and the sea-level equation (45) simplifies to

$$\delta S_j^i = -\Delta S_{j-1}^{i=\infty} + \Delta \mathcal{SL}_j^{i-1}\left(\begin{matrix}\delta I_m \\ {\scriptstyle 0\le m\le j}\end{matrix}; \begin{matrix}\delta S_m^{i=\infty} \\ {\scriptstyle 0\le m< j}\end{matrix}; \delta S_j^{i-1}\right) C_p + \frac{\Delta\Phi_j^{i-1}}{g} C_p. \tag{A8}$$

Note that because the ocean function is fixed to the present-day field, the k-iteration to determine the initial topography is not required, and the k index has therefore been dropped. We also update (46) to

$$\frac{\Delta\Phi_j^{i-1}}{g} = -\frac{1}{A_p}\frac{\rho_{\rm I}}{\rho_{\rm W}}\int\!\!\int_\Omega \Delta I_j d\Omega - \frac{1}{A_p}\int\!\!\int_\Omega \Delta \mathcal{SL}_j^{i-1}\left(\begin{matrix}\delta I_m \\ {\scriptstyle 0\le m\le j}\end{matrix}; \begin{matrix}\delta S_m^{i=\infty} \\ {\scriptstyle 0\le m< j}\end{matrix}; \delta S_j^{i-1}\right) C_p\, d\Omega, \tag{A9}$$

where A_p is given by (A6).

The first guess to the change in ocean height is given by the eustatic rise illustrated in Fig. 3(a). This is just the $i = 0, k = 1$ case discussed in the last section,

$$\delta S_j^{i=0} = -\frac{\rho_{\rm I}}{\rho_{\rm W}}\frac{C_p}{A_p}\int\!\!\int_\Omega \delta I_j\, d\Omega. \tag{A10}$$

APPENDIX B: LOVE NUMBER THEORY FOR COMPUTING $\Delta\mathcal{SL}$

This appendix provides a very brief review of the calculation of spherical harmonic coefficients of the spatially variable component of global sea-level change, $\Delta\mathcal{SL}$, using viscoelastic Love number theory. The theory is applicable to spherically symmetric models only, and we begin with the equations for a non-rotating earth.

B1 Non-rotating earth model

For a spherically symmetric, viscoelastic, non-rotating earth, geophysical observables of interest may be calculated via the space-time convolution of the appropriate viscoelastic Green's function with the surface mass load. For scalar quantities, we can write

$$\Delta\chi(\theta, \psi, t) = \int_{-\infty}^{t}\int\!\!\int_\Omega \Delta L(\theta', \psi', t')\cdot GF(\gamma, t - t')\, d\Omega'\, dt', \tag{B1}$$

where GF is the Green's function associated with observable $\Delta\chi$ and γ is the angular distance from (θ, ψ) to (θ', ψ') given by

$$\cos\gamma = \cos\theta\cos\theta' + \sin\theta\sin\theta'\cos(\psi - \psi'). \tag{B2}$$

The surface load is specified by $\Delta L(\theta, \psi, t_j) = \rho_{\rm W}\Delta S(\theta, \psi, t_j) + \rho_{\rm I}\Delta I^*(\theta, \psi, t_j)$. To calculate the change in sea level, we require expressions for the perturbations to the spatially varying component of the geoid and the solid surface, $\Delta\mathcal{G}$ and ΔR. Following (B1), we have

$$\Delta\mathcal{G}(\theta, \psi, t) = \int_{-\infty}^{t}\int\!\!\int_\Omega \Delta L(\theta', \psi', t')\frac{\phi(\gamma, t - t')}{g}\, d\Omega'\, dt', \tag{B3}$$

and

$$\Delta R(\theta, \psi, t) = \int_{-\infty}^{t}\int\!\!\int_\Omega \Delta L(\theta', \psi', t')\Gamma(\gamma, t - t')\, d\Omega'\, dt', \tag{B4}$$

where ϕ and Γ are the gravitational potential perturbation and radial displacement Green's functions, respectively. Using (B3) and (B4), (10) can be written as

$$\Delta\mathcal{SL}(\theta, \psi, t_j) = \int_{-\infty}^{t_j}\int\!\!\int_\Omega \Delta L(\theta', \psi', t')\left[\frac{\phi(\gamma, t_j - t')}{g} - \Gamma(\gamma, t_j - t')\right] d\Omega'\, dt'. \tag{B5}$$

The viscoelastic Green's functions may be expressed in terms of the non-dimensional surface load Love numbers. In the time domain, the k and h surface load Love numbers have the following normal mode form (Peltier 1974; Tromp & Mitrovica 1999),

$$\begin{aligned} k_\ell(t) &= k_\ell^E\delta(t) + \sum_{k=1}^{K} r_k'^{\ell} e^{-s_k^\ell t} \\ h_\ell(t) &= h_\ell^E\delta(t) + \sum_{k=1}^{K} r_k^{\ell} e^{-s_k^\ell t}, \end{aligned} \tag{B6}$$

where the $\delta(t)$ is the Dirac-delta function. The Green's functions ϕ and Γ are given by (Mitrovica & Peltier 1989)

$$\phi(\gamma, t) = \frac{ag}{M_e}\sum_{\ell=0}^{\infty}\left[\delta(t) + k_\ell^E\delta(t) + \sum_{k=1}^{K} r_k'^{\ell} e^{-s_k^\ell t}\right] P_\ell(\cos\gamma) \tag{B7}$$

$$\Gamma(\gamma, t) = \frac{a}{M_e} \sum_{\ell=0}^{\infty} \left[h_\ell^E \delta(t) + \sum_{k=1}^{K} r_k^\ell e^{-s_k^\ell t} \right] P_\ell(\cos\gamma) \tag{B8}$$

where a and M_e are the radius and mass of the Earth, respectively, and P_ℓ is the Legendre polynomial at degree ℓ. Applying (B7) and (B8) to (B5) yields

$$\Delta\mathcal{SL}(\theta, \psi, t_j) = \frac{a}{M_e} \int_{-\infty}^{t_j} \iint_\Omega \Delta L(\theta', \psi', t') \times \sum_{\ell=0}^{\infty} \left[\left(1 + k_\ell^E - h_\ell^E\right) \delta(t_j - t') + \sum_{k=1}^{K} \left(r_k'^\ell - r_k^\ell\right) e^{-s_k^\ell (t_j - t')} \right] P_\ell(\cos\gamma)\, d\Omega'\, dt'. \tag{B9}$$

If we model the surface load history, $\Delta L(\theta, \psi, t)$, as a series of $N + 1$ Heaviside load increments,

$$\Delta L(\theta, \psi, t) = \sum_{n=0}^{N} \left[\rho_{\mathrm{i}} \delta I_n^*(\theta, \psi) + \rho_{\mathrm{w}} \delta S_n(\theta, \psi) \right] H(t - t_n), \tag{B10}$$

where

$$H(t - t_n) = \begin{cases} 0 & \text{if } t < t_n \\ 1 & \text{if } t \geq t_n, \end{cases} \tag{B11}$$

then we may solve the temporal convolutions analytically:

$$\Delta\mathcal{SL}(\theta, \psi, t_j) = \frac{a}{M_e} \sum_{\ell=0}^{\infty} E_\ell \iint_\Omega \left[\rho_{\mathrm{i}} \Delta I_j^*(\theta', \psi') + \rho_{\mathrm{w}} \Delta S_j(\theta', \psi') \right] P_\ell(\cos\gamma)\, d\Omega' + \frac{a}{M_e} \sum_{\ell=0}^{\infty} \sum_{n=0}^{N} H(t_j - t_n) \beta(\ell, t_n, t_j) \iint_\Omega \left[\rho_{\mathrm{i}} \delta I_n^*(\theta', \psi') + \rho_{\mathrm{w}} \delta S_n(\theta', \psi') \right] P_\ell(\cos\gamma)\, d\Omega', \tag{B12}$$

where we have used the short form notation $\Delta I^*(\theta, \psi, t_j) = \Delta I_j^*(\theta, \psi)$ and $\Delta S(\theta, \psi, t_j) = \Delta S_j(\theta, \psi)$ and

$$E_\ell = 1 + k_\ell^E - h_\ell^E \tag{B13}$$

and

$$\beta(\ell, t_n, t_j) = \sum_{k=1}^{K} \frac{r_k'^\ell - r_k^\ell}{s_k^\ell} \left[1 - e^{-s_k^\ell (t_j - t_n)} \right]. \tag{B14}$$

The spatial convolutions in (B12) can also be performed spectrally by making use of the addition theorem of spherical harmonics. For a general field $\chi(\theta, \psi)$, we can write

$$\iint_\Omega \chi(\theta', \psi') P_\ell(\cos\gamma)\, d\Omega' = \frac{4\pi a^2}{2\ell + 1} \sum_{m=-\ell}^{\ell} \chi_{\ell m} Y_{\ell m}(\theta, \psi), \tag{B15}$$

where we have used the normalization (61). Applying this equation to (B12), and defining

$$T_\ell = \frac{4\pi a^3}{M_e(2\ell + 1)} \tag{B16}$$

yields

$$\Delta\mathcal{SL}(\theta, \psi, t_j) = \sum_{\ell,m} T_\ell E_\ell \left[\rho_{\mathrm{i}} \Delta I_{\ell m}^*(t_j) + \rho_{\mathrm{w}} \Delta S_{\ell m}(t_j) \right] Y_{\ell m}(\theta, \psi) + \sum_{\ell,m} T_\ell \sum_{n=0}^{j-1} \beta(\ell, t_n, t_j) \left[\rho_{\mathrm{i}} \delta I_{\ell m}^*(t_n) + \rho_{\mathrm{w}} \delta S_{\ell m}(t_n) \right] Y_{\ell m}(\theta, \psi). \tag{B17}$$

Adding the appropriate iteration counters, the spectral components required in the application of the numerical algorithm summarized in Fig. 4 are given by

$$[\Delta\mathcal{SL}_{\ell m}(t_j)]^{i-1,k} = T_\ell E_\ell \left(\rho_{\mathrm{i}} \left[\Delta I_{\ell m}^*(t_j) \right]^{k-1} + \rho_{\mathrm{w}} \left[\Delta S_{\ell m}(t_{j-1}) \right]^{i=\infty,k} + \rho_{\mathrm{w}} \left[\delta S_{\ell m}(t_j) \right]^{i-1,k} \right) + T_\ell \sum_{n=0}^{j-1} \beta(\ell, t_n, t_j) \left(\rho_{\mathrm{i}} \left[\delta I_{\ell m}^*(t_n) \right]^{k-1} + \rho_{\mathrm{w}} \left[\delta S_{\ell m}(t_n) \right]^{i=\infty,k} \right). \tag{B18}$$

B2 Rotating earth model

Changes in the surface mass (ice plus ocean) load will drive perturbations in the Earth's rotation vector, and these perturbations will, in turn, influence global sea level (e.g. Han & Wahr 1989; Milne & Mitrovica 1996, 1998b). In this section, we review the theory required to augment (B18) to include rotation effects.

Normal mode theories have been developed for computing surface load-induced changes in the magnitude and orientation of the rotation vector on spherically symmetric, viscoelastic earth models. A new derivation, which corrects inaccuracies in previous work, is found in Mitrovica *et al.* (2005). The computed changes in the rotation vector lead to an evolving centrifugal potential, and the perturbation in this potential from the equilibrium value (i.e. from the value prior to loading, $t = t_0$ in our nomenclature) is known as the 'rotational potential perturbation' or the 'driving potential'. We will denote the driving potential as $\Delta\Lambda(\theta, \psi, t_j)$, and remind the reader that this field is a function of all the ice and ocean load increments from t_0 to t_j.

Since the driving potential is comprised of the difference between two ellipsoidal forms of distinct amplitude and orientation, the spherical harmonic coefficients of the potential are non-zero at degree zero and two only, and we can write (e.g. Milne & Mitrovica 1998b)

$$\Delta\Lambda(\theta, \psi, t_j) = \Delta\Lambda_{0,0}(t_j)Y_{0,0}(\theta, \psi) + \sum_{m=-2}^{2} \Delta\Lambda_{2,m}(t_j)Y_{2,m}(\theta, \psi). \tag{B19}$$

The mapping between perturbations in the rotation vector and the harmonic coefficients appearing in (B19) is given in Milne & Mitrovica (1998b). For small perturbations in the rotation vector, the driving potential will be dominated by a degree two and order one 'quadrential' geometry associated with polar wander effects (e.g. Han & Wahr 1989; Milne & Mitrovica 1998b).

The spherical harmonic coefficients of the sea-level perturbation associated with this potential loading may be computed via a time convolution of the coefficients in the driving potential with degree dependent viscoelastic tidal Green's functions

$$\Delta\mathcal{SL}^T_{\ell m}(t_j) = \int_{-\infty}^{t_j} \Delta\Lambda_{\ell m}(t') \left[\frac{\phi^T_\ell(t_j - t')}{g} - \Gamma^T_\ell(t_j - t') \right] dt'. \tag{B20}$$

The superscript T denotes quantities associated with a tidal effective (or potential) forcing. If, in analogy with the surface mass load Love numbers, we introduce the non-dimensional tidal (or tidal effective) Love numbers (Peltier 1976) as

$$\begin{aligned} k^T_\ell(t) &= k^{T,E}_\ell \delta(t) + \sum_{k=1}^{K} r'^{\ell,T}_k e^{-s^\ell_k t} \\ h^T_\ell(t) &= h^{T,E}_\ell \delta(t) + \sum_{k=1}^{K} r^{\ell,T}_k e^{-s^\ell_k t}, \end{aligned} \tag{B21}$$

then the Green's functions $\phi^T_\ell(t)$ and $\Gamma^T_\ell(t)$ are simply given by (Milne & Mitrovica 1998b)

$$\phi^T_\ell(t) = \delta(t) + k^T_\ell(t) \tag{B22}$$

$$\Gamma^T_\ell(t) = \frac{1}{g} h^T_\ell(t), \tag{B23}$$

where the Dirac-delta function incorporates the direct effect of the potential forcing. If we furthermore adopt the approach in (B10) and express the driving potential in terms of a series of discrete Heaviside increments as

$$\Delta\Lambda_{\ell m}(t) = \sum_{n=0}^{N} \delta\Lambda_{\ell m}(t_n) H(t - t_n), \tag{B24}$$

then, using (B20)–(B24), we can write

$$\Delta\mathcal{SL}^T_{\ell m}(t_j) = \frac{1}{g} E^T_\ell \Delta\Lambda_{\ell m}(t_j) + \frac{1}{g} \sum_{n=0}^{j-1} \beta^T(\ell, t_n, t_j)\, \delta\Lambda_{\ell m}(t_n), \tag{B25}$$

where

$$E^T_\ell = 1 + k^{T,E}_\ell - h^{T,E}_\ell \tag{B26}$$

and

$$\beta^T(\ell, t_n, t_j) = \sum_{k=1}^{K} \frac{r'^{\ell,T}_k - r^{\ell,T}_k}{s^\ell_k} \left[1 - e^{-s^\ell_k (t_j - t_n)} \right]. \tag{B27}$$

Using (B25) we can augment (B18) to read

$$\begin{aligned} [\Delta\mathcal{SL}_{\ell m}(t_j)]^{i-1,k} = {} & T_\ell E_\ell \left(\rho_{\rm I} \left[\Delta I^*_{\ell m}(t_j) \right]^{k-1} + \rho_{\rm W} [\Delta S_{\ell m}(t_{j-1})]^{i=\infty,k} + \rho_{\rm W} [\delta S_{\ell m}(t_j)]^{i-1,k} \right) \\ & + T_\ell \sum_{n=0}^{j-1} \beta(\ell, t_n, t_j) \left(\rho_{\rm I} \left[\delta I^*_{\ell m}(t_n) \right]^{k-1} + \rho_{\rm W} [\delta S_{\ell m}(t_n)]^{i=\infty,k} \right) \\ & + \frac{1}{g} E^T_\ell \left([\Delta\Lambda_{\ell m}(t_{j-1})]^{i=\infty,k} + [\delta\Lambda_{\ell m}(t_j)]^{i-1,k} \right) \\ & + \frac{1}{g} \sum_{n=0}^{j-1} \beta^T(\ell, t_n, t_j) [\delta\Lambda_{\ell m}(t_n)]^{i=\infty,k}. \end{aligned} \tag{B28}$$

The coefficients $\delta\Lambda_{\ell m}(t_n)$ ($n = 0$, $j - 1$) are computed using all the ice load increments (up to $j - 1$) computed over the previous iteration through the full glacial cycle ($[\delta I^*_{\ell m}(t_n)]^{k-1}$) and the ocean load increments (up to $j - 1$) computed from the converged solutions during the kth iteration through the full glacial cycle ($[\delta S_{\ell m}(t_n)]^{i=\infty,k}$). In contrast, the total perturbation $[\Delta\Lambda_{\ell m}(t_j)]^{i-1,k}$ is computed using the load coefficients $[\Delta I^*_{\ell m}(t_j)\ ]^{k-1}$, $[\Delta S_{\ell m}(t_{j-1})]^{i=\infty,k}$, and $[\delta S_{\ell m}(t_j)]^{i-1,k}$. The last of these sets of load coefficients is being iteratively improved within the inner i-loop iteration, and thus the driving potential will be iteratively improved within both the inner and outer iteration loops. That is, as the load is being revised, either within the ith or kth iteration loop, a prediction of the perturbation to the rotation vector and the associated driving potential are also being revised and implemented in (B28).

In deriving (B28), we independently treated contributions to the sea-level change from surface mass loading (B18) and rotation effects and then we added these contributions to derive the RHS of that equation. This procedure was adopted to highlight the distinct physics of these contributions, and for the purpose of clarity; but we could have derived the same equation by introducing both contributions at the outset. In any event, it is important to emphasize that the two contributions are coupled through the LHS of (B28). For example, changes in rotation will perturb predictions of sea-level change, and this perturbation will, in turn, impact load-induced contributions to the sea level, and so on.